JOURNAL OF PETROLOGY | VOLUME 41 | NUMBER 2 | PAGES 175–200 | 2000

# Cooling History and Exhumation of Lower-Crustal Granulite and Upper Mantle (Malenco, Eastern Central Alps)

**OTHMAR MÜNTENER*, JÖRG HERMANN† AND VOLKMAR TROMMSDORFF**

INSTITUT FÜR MINERALOGIE UND PETROGRAPHIE, ETH ZÜRICH, CH 8092 ZÜRICH, SWITZERLAND

**RECEIVED JULY 30, 1998; REVISED TYPESCRIPT ACCEPTED JULY 8, 1999**

*The Braccia gabbro of Val Malenco, Italian Alps, intruded 275 My ago during Early Permian lithospheric extension. The intrusion took place along the crust–mantle transition zone and caused granulite metamorphism of lower-crustal and upper-mantle rocks. The magmatic crystallization of the gabbro was outlasted by ductile deformation, which is also observed in the other rocks of the crust–mantle transition. Two stages of retrograde metamorphism followed. Mineral parageneses in garnet–kyanite gneiss, metagabbro, and metaperidotite record a first stage of near-isobaric cooling under anhydrous conditions. The stabilized crust–mantle transition then persisted over a period of about 50 My into the Late Triassic. Exhumation of the crust–mantle complex began with the onset of continental rifting during Early Jurassic. This stage of retrograde metamorphism is recorded by near-isothermal decompression and partial hydration of the granulitic mineral assemblages. The whole crust-to-mantle complex was then exposed in the Tethyan ocean near its Adriatic margin. The magmatic assemblage of the Braccia gabbro formed at 1–1·2 GPa and 1150–1250°C. Microstructures show that the gabbroic rocks evolved from olivine gabbros through spinel to garnet granulite whereas the peridotites recrystallized within the spinel peridotite field and the pelitic granulites remained in the stability field of kyanite. Such an evolution is characteristic of isobaric cooling after magmatic underplating. Granulitic mineral assemblages record cooling from 850°C to 650°C with decompression to 0·8 ± 0·1 GPa, and* $dP/dT < \sim 0{\cdot}15$ *GPa/100°C. During later hydration, Cl-rich amphibole and biotite + plagioclase formed in the gabbros, clinozoisite + phengite + paragonite ± staurolite ± chloritoid in the metapelites and olivine + tremolite + chlorite ± talc in the ultramafic rocks at metamorphic conditions of 0·9 ± 0·1 GPa and 600 ± 50°C. Subsequent retrograde metamorphism involved decompression of ∼0·3 GPa and cooling to ∼500°C, consistent with the preservation of the olivine + tremolite + talc assemblage in ultramafic rocks. Estimated uplift rates of 1–2 mm/year indicate a 15–30 My exhumation related to Jurassic rifting. The two-stage retrograde path of the Malenco granulites separated by >50 My suggests that Permian extension and Jurassic rifting are two independent tectonic processes. The presence of hydrous, Cl-rich minerals at 600 ± 50°C and 0·8 ± 0·1 GPa requires input of externally derived fluids at the base of 30 km thick continental crust into previously dry granulites at the onset of Jurassic rifting. These fluids were generated by dehydration of continental crust juxtaposed during rifting with the hot, exhuming granulite complex along a active shear zone.*

KEY WORDS: *subcontinental lithospheric mantle; granulite; continental rifting; retrograde metamorphism; Malenco*

## INTRODUCTION

In recent years, a great number of petrologic studies have been carried out to determine the tectonic environment of granulite formation (e.g. Bohlen, 1987, 1991; Fountain, 1989; Harley, 1989; Rudnick & Fountain, 1995). Harley (1989) proposed that the origin of granulites can be interpreted on the basis of their *P–T* paths. He distinguished between isothermally decompressed (ITD) and isobarically cooled (IBC) granulites. IBC granulites are regarded as products of mafic underplating (e.g. Bohlen, 1991) and are interpreted as true lower crust (Rudnick

*Corresponding author. Present address: Woods Hole Oceanographic Institution, Woods Hole, MA 02543, USA. Telephone: 708-289-3248. Fax: 708-457-2183. e-mail: omuentener@whoi.edu
†Present address: Research School of Earth Sciences, ANU Canberra, A.C.T. 0200, Australia.

& Fountain, 1995). However, many of the granulite terrains that are considered as true lower crust are not associated with a large mass of subcontinental upper-mantle rocks. For example, the Ivrea zone in northern Italy is one of the largest lower-crustal sections in the world, but the associated upper-mantle rocks are small lenses and may not represent the uppermost continental mantle (Quick *et al.*, 1995). In this paper, $P$–$T$ data are presented for an exposed section from the lowermost continental crust to the uppermost subcontinental mantle in the Eastern Central Alps, in which mafic underplating occurred in Permian times (Müntener & Hermann, 1996; Hermann *et al.*, 1997). These exposures provide us with the ability to test tectonic concepts of isobarically cooled granulites.

Exhumation of granulite-facies lower-crustal rocks and subcontinental peridotites is an important process, because the presence of such rocks along passive continental margins potentially provides information about how rifting processes operated in deeper parts of the lithosphere. The petrologic characterization of exposed lower-crustal and upper-mantle rocks is crucial for the interpretation of geophysical data of modern passive continental margins, and hence for the development of tectonic models of rifting. Although there is increasing evidence from the Alps and from deep-sea drilling studies that subcontinental peridotites were exhumed during rifting (Lemoine *et al.*, 1987; Piccardo *et al.*, 1990; Hoogerduijn Strating *et al.*, 1993; Trommsdorff *et al.*, 1993; Boillot *et al.*, 1995; Rampone *et al.*, 1995), the role and importance of the exposure of lower crust at passive continental margins remains unclear. This paper presents a case study from the Alps (Malenco, Italy; Fig. 1) in which lower crust (i.e. mafic and pelitic granulites) and subcontinental peridotites have been exhumed. We use microstructures and thermobarometric data to show that Permian granulites underwent anhydrous, near-isobaric cooling followed by hydrous, near-isothermal decompression and exhumation on the Tethyan sea-floor. Subsequent hydration reactions constrain rifting and uplift models. Although the study area is much smaller than the Ivrea zone and also more heavily overprinted by Alpine collisional metamorphism, it has preserved some original contacts between mantle and crustal rocks since the latest Paleozoic (Trommsdorff *et al.*, 1993; Müntener & Hermann, 1996; Hermann *et al.*, 1997). This feature is consistent with the observation that granulites and peridotites followed the same $P$–$T$ evolution from Early Permian on.

## GEOLOGICAL BACKGROUND

The Malenco area is located at the boundary between southeastern Switzerland and northern Italy (Fig. 1). The study area lies at the Penninic–Austroalpine boundary, between the Pennine crystalline nappes and the lower Austroalpine Margna nappe, which is composed of basement rocks with their Mesozoic sedimentary cover.

The lower part of the Malenco–Forno unit consists of serpentinized peridotite (the Malenco ultramafic rocks), and of minor, less serpentinized, spinel lherzolite, garnet clinopyroxenite, spinel websterite, dunite and harzburgite (Müntener & Hermann, 1996). The ultramafic rocks are overlain by continental crust that consists of kyanite–garnet gneisses with local granitoid partial melt segregations, minor calcsilicate rocks and marbles. The ultramafic and granulite-facies rocks are welded by the Braccia gabbro. The gabbro complex differentiated at the transition between continental crust and underlying mantle. It evolved from Mg to Fe gabbro to quartz diorite and highly differentiated Fe–Ti–P-rich gabbros and diorites. Several dikes of gabbro within peridotite and granulite demonstrate that the Braccia gabbro intruded mantle rocks as well as the lowermost crust (Müntener & Hermann, 1996; Hermann *et al.*, 1997). Single-zircon U–Pb data from granitoid partial melts within the pelitic granulites and the gabbro yield Permian ages that agree within the limit of uncertainty (Hansmann *et al.*, 1996; Hermann *et al.*, 1997). These data demonstrate that the Malenco rock association represents an undisturbed lower-crust to upper-mantle section, which was the crust-to-mantle transition in the Permian. The regional geology, field relations, rock types, and a detailed map of the study area have been presented by Müntener & Hermann (1996).

In the western part of the Malenco unit, the ultramafic rocks are cut by ophicarbonate zones and by mid-ocean-ridge-like basaltic dikes of the Forno 'ophiolite' suite (Fig. 1). Rodingitization of mafic dikes and ophicarbonate breccias bears a marine stable isotope signature (Burkhard & O'Neill, 1988; Pozzorini & Früh-Green, 1996) indicating that metamorphism and metasomatism took place in an oceanic environment. The Forno unit itself consists of metamorphosed basalt with locally preserved pillow lavas and breccias (Montrasio, 1973), which are overlain by a metasedimentary sequence of presumably Jurassic age (Peretti, 1985). In Jurassic time, the Margna, Malenco and Forno units formed the transition from the Adriatic continental margin to the Piemont Ligurian ocean, with a geometry similar to the present-day margin of Galicia (e.g. Boillot *et al.*, 1995). The Malenco ultramafic rocks were a denuded subcontinental mantle fragment of the Adria lithosphere (Trommsdorff *et al.*, 1993; Hermann & Müntener, 1996).

The geological background provides rigid boundary conditions on the pre-Alpine retrograde metamorphic evolution of the studied rocks: (1) the rocks represent a former crust-to-mantle transition and thus peridotites, gabbros and pelitic granulites must have a common

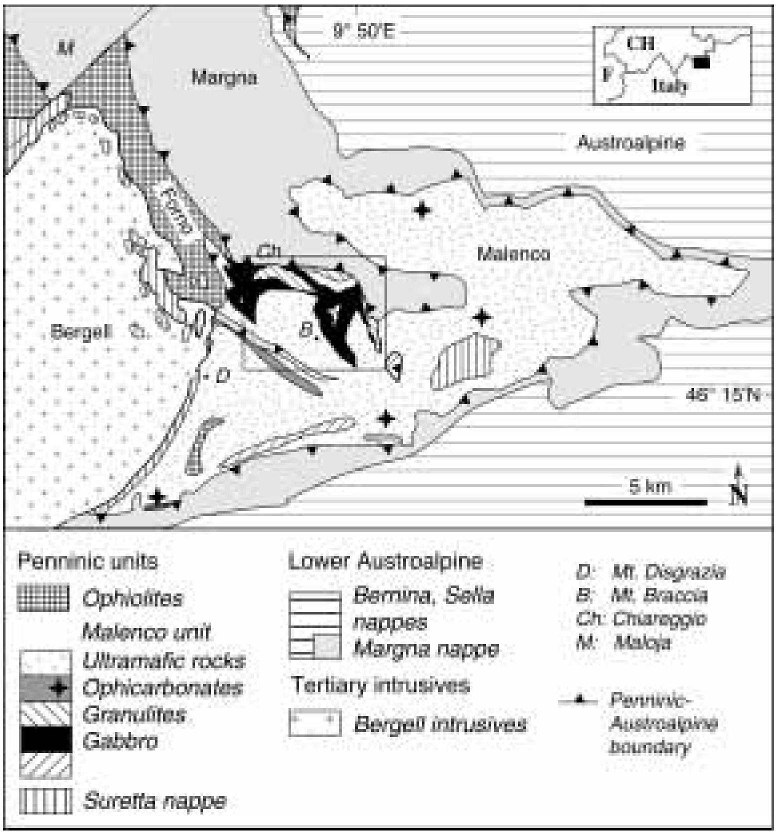


**Fig. 1.** Outline tectonic map of the Penninic–Austroalpine boundary in Val Malenco (northern Italy). Inset in the upper right corner shows the location of the study area in the Eastern Central Alps. Frame outlines Fig. 2, where rocks with pre-Alpine parageneses are exposed.

evolution; (2) the Permian crystallization age of the Braccia gabbro (Hansmann *et al.*, 1996) indicates that the retrograde metamorphism is younger than Permian; (3) the rocks were exhumed in Jurassic time and were situated at the Adriatic continental margin.

During the Alpine orogeny, the Malenco unit was incorporated into the Alpine nappe stack during the Upper Cretaceous (Müntener *et al.*, 1997), and most of the samples recrystallized under Alpine epidote–amphibolite-facies conditions (about 0·5–0·7 GPa and 450–500°C: Guntli & Liniger, 1989; Hermann, 1997). Despite this Alpine metamorphism, several lenses around Mt Braccia (Fig. 2) preserved pre-Alpine, high-grade assemblages that allow study of the pre-Alpine metamorphic evolution of the Malenco rocks.

## PETROGRAPHY OF PRE-ALPINE METAMORPHIC ASSEMBLAGES

The succession of pre-Alpine mineral assemblages shows a clear order of decreasing metamorphic grade (Tables 1–3). Textures and mineral compositions allow a clear distinction of assemblages produced by Alpine metamorphic overprinting of pre-Alpine assemblages. Pre-Alpine minerals are found within areas of minor Alpine deformation and hence minor fluid access (Fig. 2).

### Textures related to the retrograde metamorphism of the Braccia gabbro

The major primary minerals of the Braccia gabbro are two pyroxenes and plagioclase, with minor and variable amounts of olivine, Ti-pargasite, spinel and ilmenite. Retrograde reactions were initially anhydrous, but were followed by hydrous recrystallization. Coronas with anhydrous assemblages are consistently developed between olivine and plagioclase. However, because olivine is a minor phase, there are only a few samples with well-developed anhydrous coronas. Coronas with hydrous assemblages occur in all gabbros and are found between ilmenite and plagioclase, and pyroxene and plagioclase, respectively.

#### *Granoblastic equilibration*

After crystallization the magmatic assemblage of the Braccia gabbro underwent ductile deformation and

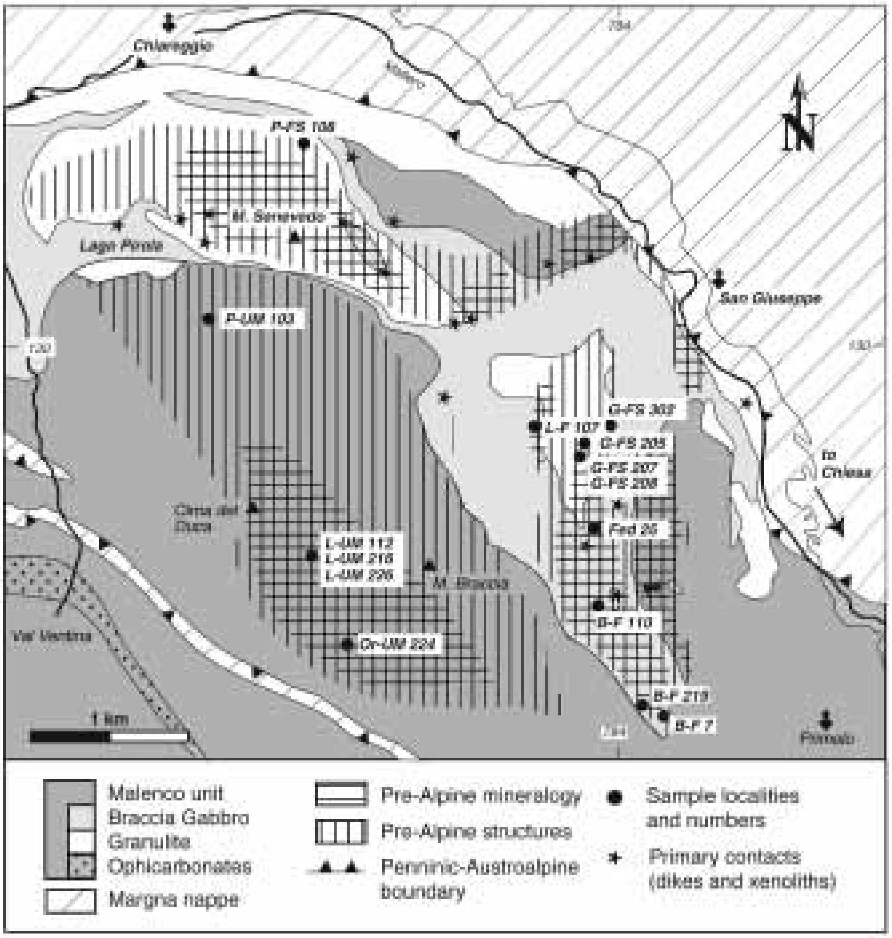


**Fig. 2.** Simplified geologic map of the study area, modified after Müntener & Hermann (1996). Pattern for pre-Alpine mineralogy refers to areas with granulite-facies rocks. Locations of samples reported in this study are indicated by dots.

recrystallization under granulite-facies conditions. Most of the minerals now form polygonal granoblasts which partly replaced magmatic textures (Fig. 3a). Granoblasts lack compositional zoning, which is evidence for equilibrium during granulite-facies metamorphism.

*Spinel–two-pyroxene coronas*

Typical features of the coronas between olivine and plagioclase are: (1) small neoblasts of orthopyroxene, clinopyroxene and spinel, which are found between olivine and plagioclase grains (Fig. 3b); orthopyroxene, the most abundant phase, borders the olivine grains; (2) pyroxene grains contain abundant, micrometer-scale inclusions of wormy spinel (Fig. 3b), which formed by subsolidus co-precipitation of spinel and pyroxene, rather than by exsolution of spinel from Al-rich pyroxene. In gabbros with olivine and ilmenite, spinel + pyroxene-bearing coronas are also present around ilmenite.

*Garnet–two-pyroxene coronas*

Two-pyroxene + spinel corona structures show overgrowths of two-pyroxene + garnet corona structures. Garnet grains occur either as subidioblastic single grains, which are in contact with orthopyroxene and clinopyroxene next to plagioclase, or as anhedral–poikilitic grains that enclose vermicular spinel (Fig. 3b). Such coronas are typical of many metagabbros and mafic granulites and are thought to be formed by solid-state reactions along retrograde, near-isobaric cooling paths (e.g. Griffin & Heier, 1973; Whitney & McLelland, 1973; Johnson & Carlson, 1990).

*Garnet amphibole coronas*

In some olivine gabbros, the anhydrous coronas are overgrown by ones that contain amphibole + garnet (Fig. 3b). These coronas are found at the contacts between spinel + garnet coronas and plagioclase that contains

*Table 1: Mineral assemblages in the Braccia gabbro; numbers refer to different generations of minerals given in Table 4*

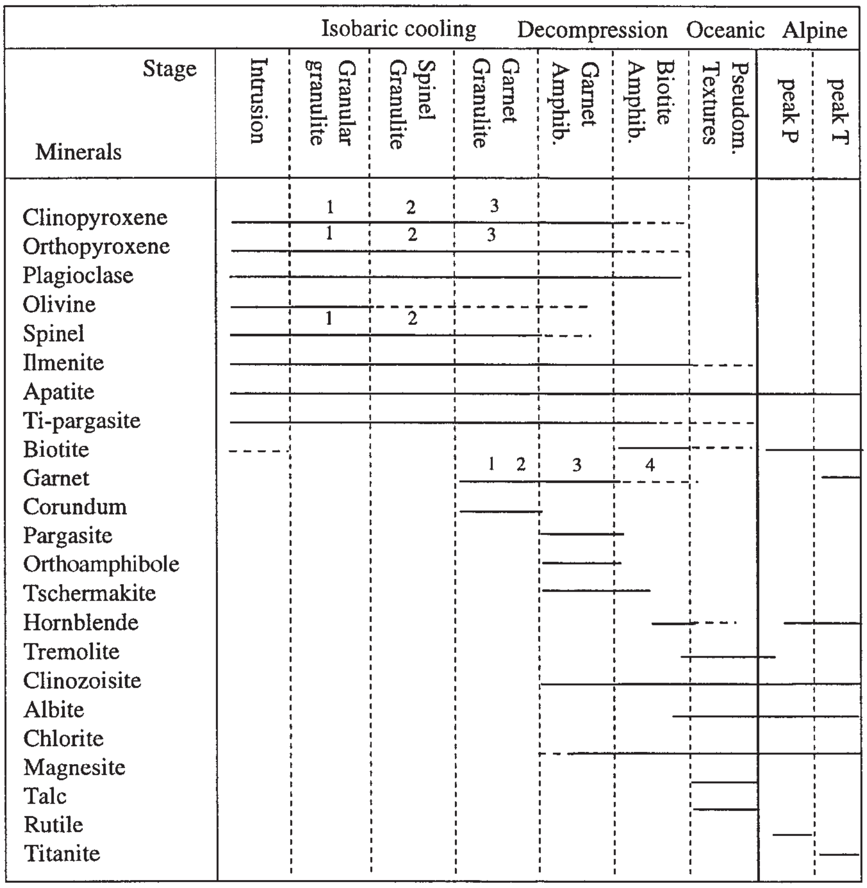


acicular inclusions of clinozoisite. Amphibole needles have clearly overgrown clino- and orthopyroxene. Idiomorphic garnet, which is rarely found in the corona amphibole matrix, shows straight grain boundaries (Fig. 3b).

*Biotite amphibole coronas*

Coronas of amphibole + biotite separate plagioclase from ilmenite, Ti-pargasite and biotite in Fe-rich metagabbros. The corona minerals are in textural equilibrium with plagioclase and clinozoisite. In gabbros that display garnet + amphibole coronas, some garnet grains are overgrown by biotite, which indicates that the latter mineral is part of a later-stage corona. However, biotite, amphibole and garnet appear to be in textural equilibrium in some coronas in ilmenite-rich metagabbros (Fig. 3c).

*Pseudomorphic textures related to low-grade hydration*

Pseudomorphic replacement of pyroxene by a fine-grained aggregate of amphibole is pre-Alpine, but it postdates the formation of biotite + amphibole coronas, which form a continuous network along former grain boundaries of pyroxene and plagioclase (Fig. 3d). Some olivine grains have been replaced by tremolite and talc. In rocks with only weak Alpine deformation, fine-grained amphibole is surrounded by amphibole grains that are aligned in the Alpine foliation. This is evidence of the pre-Alpine nature of pseudomorphic replacement of pyroxenes by amphibole.

## Textures related to the retrograde metamorphism of the Malenco peridotite

The Malenco peridotite equilibrated under conditions of the spinel peridotite facies before the intrusion of the Braccia gabbro (Müntener, 1997). Its early retrograde mineral assemblages are mainly anhydrous. With the ingress of fluid, original contacts among olivine, spinel and pyroxene have been overgrown and partly replaced by coronas that contain hydrous phases, which are described in this section.

*Table 2: Mineral assemblages in the Malenco peridotite; numbers refer to different generations of minerals given in Table 5*

| | | Isobaric cooling | Decompression | Oceanic | Alpine |
|---|---|---|---|---|---|
| Stage / Minerals | Mantle paragenesis | Granulite | Coronas and pseudomorphs | pseudo-morphs | |
| Olivine | 1 | 2 | 3 | | — |
| Clinopyroxene | 1 | 2 | | | — |
| Orthopyroxene | 1 | 2 | 3 | | |
| Spinel | 1 | 2 | | | |
| Ti-pargasite | 1 | 2 | | | |
| Mg-Hornblende | | — | — | | |
| Chromite | | | — | | |
| Talc | | | — - - - | - - - | |
| Tremolite | | | 1 2 | - - - | |
| Chlorite | | | — | — | — |
| Ferrichromite | | | — | | |
| Ilmenite | | - - - | — | — | — |
| Antigorite | | | | | — |
| Chrysotile/Lizardite | | | | — | |
| Magnetite | | | | — | — |
| Brucite | | | | — | - - - |
| Ti-clinohumite | | | | - - - | — |
| Calcite | | | | — | — |

*Table 3: Mineral assemblages in pelitic granulite; numbers refer to different generations of minerals given in Table 6*

| | Pre-Alpine | | | Alpine |
|---|---|---|---|---|
| Stage / Minerals | Granulite | Anhydrous recrystallization | Hydrous re-crystallization | Alpine Metamorphism |
| Garnet | 1 | 2 3 | 4 | — |
| Quartz | — | — | — | — |
| Biotite | 1 | 2 | 3 | — |
| Plagioclase | — | — | - - - | |
| Kyanite | 1 | 2 | 3 - - - | |
| Ilmenite | — | — - - - | | |
| Rutile | | - - - — | — | |
| Staurolite | | | — | |
| Chloritoid | | | — | |
| Paragonite | | | — | |
| Clinozoisite | | | — | — |
| Albite | | | - - - — | — |
| Phengite | | | — | — |
| Muscovite | | | — | — |
| Chlorite | | | - - - — | — |
| Stilpnomelane | | | | — |
| Titanite | | | | — |
| Fe-oxide | | | | — |

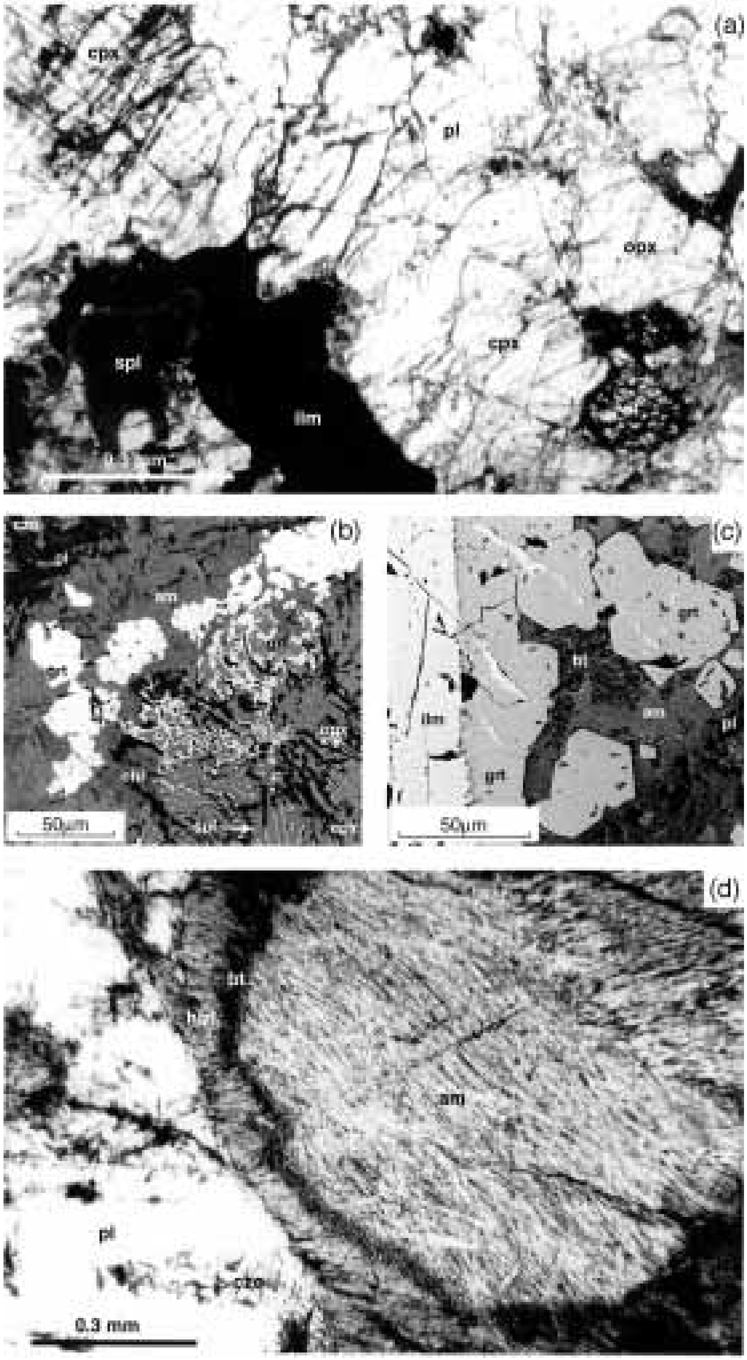


**Fig. 3.** Photomicrographs and back-scattered electron (BSE) images of gabbro microstructures. Mineral abbreviations are after Kretz (1983). (a) 'Primary' texture of clinopyroxene (cpx), orthopyroxene (opx), plagioclase (pl), ilmenite (ilm), spinel (spl) and olivine (ol) in sample L-F 107. (b) Polyphase corona between olivine (lower right corner, outside the image) and plagioclase. The first corona consists of orthopyroxene, clinopyroxene and vermicular spinel (spinel granulite). Spinel has been replaced by garnet (grt) and two pyroxenes (garnet granulite). Between garnet + two-pyroxene coronas and plagioclase, idiomorphic garnet (grt) is in equilibrium with pargasite (garnet amphibolite). The latter always has overgrown pyroxene. Small clinozoisite (czo) needles occur within plagioclase. Sample B-F7. (c) Ilmenite is partly bordered by garnet, which shows equilibrium textures with a mixture of biotite (bt) and amphibole (am). Sample B-F219. (d) Pseudomorphic amphibole after orthopyroxene. It should be noted that the hornblende–biotite corona has been preserved. Plagioclase ($An_{50}$) contains clinozoisite needles. Sample Fed 25.

*Granoblastic equilibration*

Small neoblasts of olivine, orthopyroxene, clinopyroxene, spinel and Ti-pargasite form mortar structures around large, preexisting mantle minerals (Fig. 4a). No peridotite sample appears to have been completely recrystallized during the granoblastic equilibration. Most grain boundaries among the neoblasts are straight (Fig. 4b), and neoblastic minerals vary little in their compositions.

*Chlorite–amphibole coronas and pyroxene pseudomorphs*

The transition from anhydrous to hydrous parageneses is best recorded in the corona structures of undeformed peridotites. Depending on the microstructural site, three different corona parageneses are observed:

(1) orthopyroxene, olivine and spinel have been replaced by radial chlorite, by chromite and by amphibole in three zones (Fig. 4c). Near Al-rich spinel, a small zone of symplectitic intergrowth of chromite and chlorite (zone A) lies within a radial, monomineralic corona of chlorite (zone B). Close to orthopyroxene, chlorite occurs along with acicular tremolite (zone C).

(2) Chlorite + amphibole coronas have been found along grain boundaries between ortho- and clinopyroxene. Olivine is absent. In more hydrated rocks, these amphibole + chlorite coronas connect in a three-dimensional network around pyroxene grains.

(3) Pseudomorphic replacement of orthopyroxene by olivine + talc ± tremolite ± chlorite (Fig. 4d) post-dates the formation of amphibole + chlorite coronas. Talc is found in intergrowths with minor tremolite and chlorite.

Strongly recrystallized and deformed samples show an assemblage of olivine + amphibole + chlorite + ferrichromite ± ilmenite (Fig. 4e). Symplectites of chromite + colorless clinochlore have been replaced by ferrichromite and pale brown, Cr-rich pennine. Pseudomorphic replacement of pyroxene by olivine + amphibole post-dates the formation of chlorite + amphibole coronas, which are arranged in a network along the former grain boundaries of clino- and orthopyroxene.

*Pseudomorphic textures related to low-grade hydration*

During Alpine metamorphism, most of the peridotite was replaced by antigorite serpentinite. However, some undeformed parts of the peridotite unit preserve a texture typically found in hydrothermally altered peridotite. In such rocks, olivine has been replaced by a mesh of serpentine (Fig. 4f). Fibrous serpentine veins partly cut completely altered orthoyproxene. The centers of most such veins are filled with oxide minerals. The serpentine ± Fe-oxide assemblage was evidently recrystallized to antigorite during Alpine metamorphism (Fig. 3f). Relics of chrysotile overgrown by Alpine antigorite were reported by Mellini *et al.* (1987) in a high-resolution transmission electron microscopy (HRTEM) study of Val Malenco antigorite. The chrysotile may represent low-temperature, ocean-floor metamorphism.

## Textures related to the retrograde metamorphism of metapelites

The granulite-facies paragenesis of the metapelites consists of garnet, kyanite, plagioclase, quartz, ilmenite and minor biotite (Fig. 5a). Subsequent anhydrous recrystallization is characterized by: (1) pseudomorphs of fibrous kyanite after large kyanite grains (Fig. 5b); (2) the formation of rutile rims around ilmenite coexisting with garnet and plagioclase; (3) the large (up to 2 cm) homogeneous garnets that formed during granulite-facies metamorphism, which display a composite retrograde rim of ~0·2 mm thickness. Rarer small (0·2 mm diameter) idiomorphic garnet grains also formed during anhydrous recrystallization.

Many pelitic granulites show evidence for subsequent hydrous recrystallization. In kyanite-bearing rocks, plagioclase has been replaced by clinozoisite, paragonite and minor phengite (Fig. 5c). Contacts between garnet and kyanite have been overgrown by a fine-grained aggregate of chloritoid, paragonite and rare staurolite. Rare chloritoid forms idiomorphic needles that coexist with kyanite and paragonite (Fig. 5d). These hydrous parageneses are found only in rocks without Alpine deformation and differ from the parageneses that formed during Alpine metamorphism (Table 3).

# MINERAL CHEMISTRY

From a total of about 40 samples studied by electron microprobe, 5–11 samples per rock type were chosen for detailed mineral chemistry. They were selected on the basis of textural relationships in which pre-Alpine minerals clearly could be distinguished from Alpine metamorphic assemblages. Representative analyses are given in Tables 4–6, together with analytical procedures and mineral calculation schemes.

## Braccia gabbro

Clino- and orthopyroxene show a systematic decrease of Al and Na, and a concomitant increase in *mg*-number, which are correlated with the transition from granular granulite through spinel to garnet granulite coronas (Fig. 6). Garnet varies considerably in its composition, both between different grains and, in many cases, within single grains. For example, garnet in textural equilibrium with orthopyroxene is richer in pyrope and lower in grossular content than garnet that shows textural equilibrium with

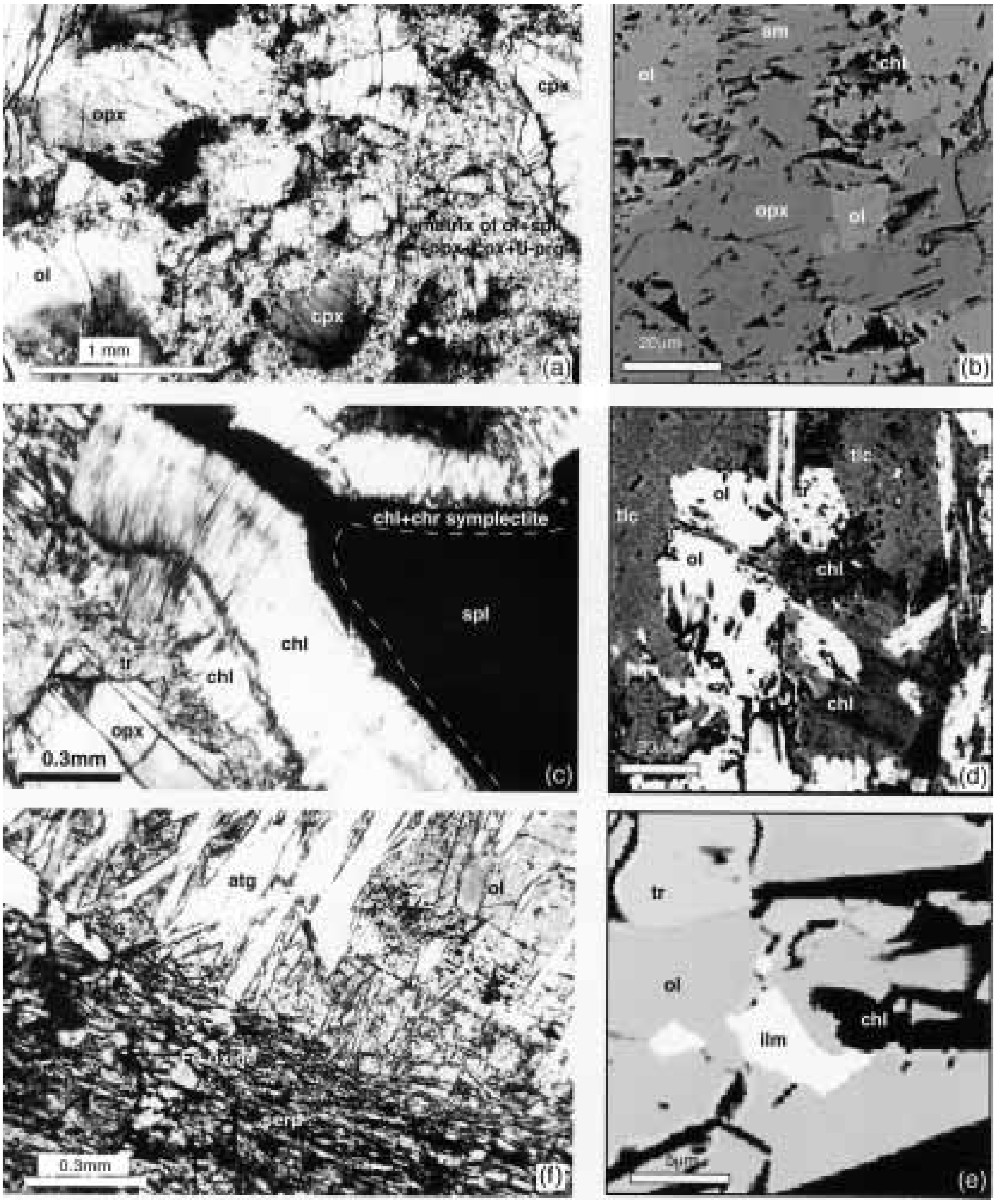


**Fig. 4.** Photomicrographs and BSE images of peridotite microstructures. (a) Porphyroclastic texture, in which large porphyroclasts of olivine, clinopyroxene, orthopyroxene and spinel are surrounded by small neoblasts of the same minerals in sample L-UM 216. (b) Textural equilibrium of olivine, orthopyroxene and clinopyroxene. Amphibole and chlorite have partly replaced neoblasts in sample L-UM 216. (c) Chlorite corona between spinel and orthopyroxene. The outermost opaque rim consists of symplectitic intergrowth of chromite and chlorite. Tremolitic amphibole has replaced orthopyroxene. It should be noted that the former orthopyroxene–spinel contact is indicated by two varieties of chlorite. Sample L-UM 112. (d) Breakdown of orthopyroxene to olivine + talc (tlc) ± chlorite ± tremolite (tr). Talc and chlorite show poorly polished surfaces. Sample L-UM 226. (e) Equilibrium texture among olivine, amphibole, chlorite and ilmenite. The coexistence of olivine and ilmenite should be noted. Sample Or-UM 224. (f) Radial antigorite (atg) that has overgrown low-grade (oceanic) serpentine (serp). Sample P-UM 103. The small oxide mineral trails included in antigorite grain should be noted ($mg$-number$_{atg}$ > $mg$-number$_{serp}$).

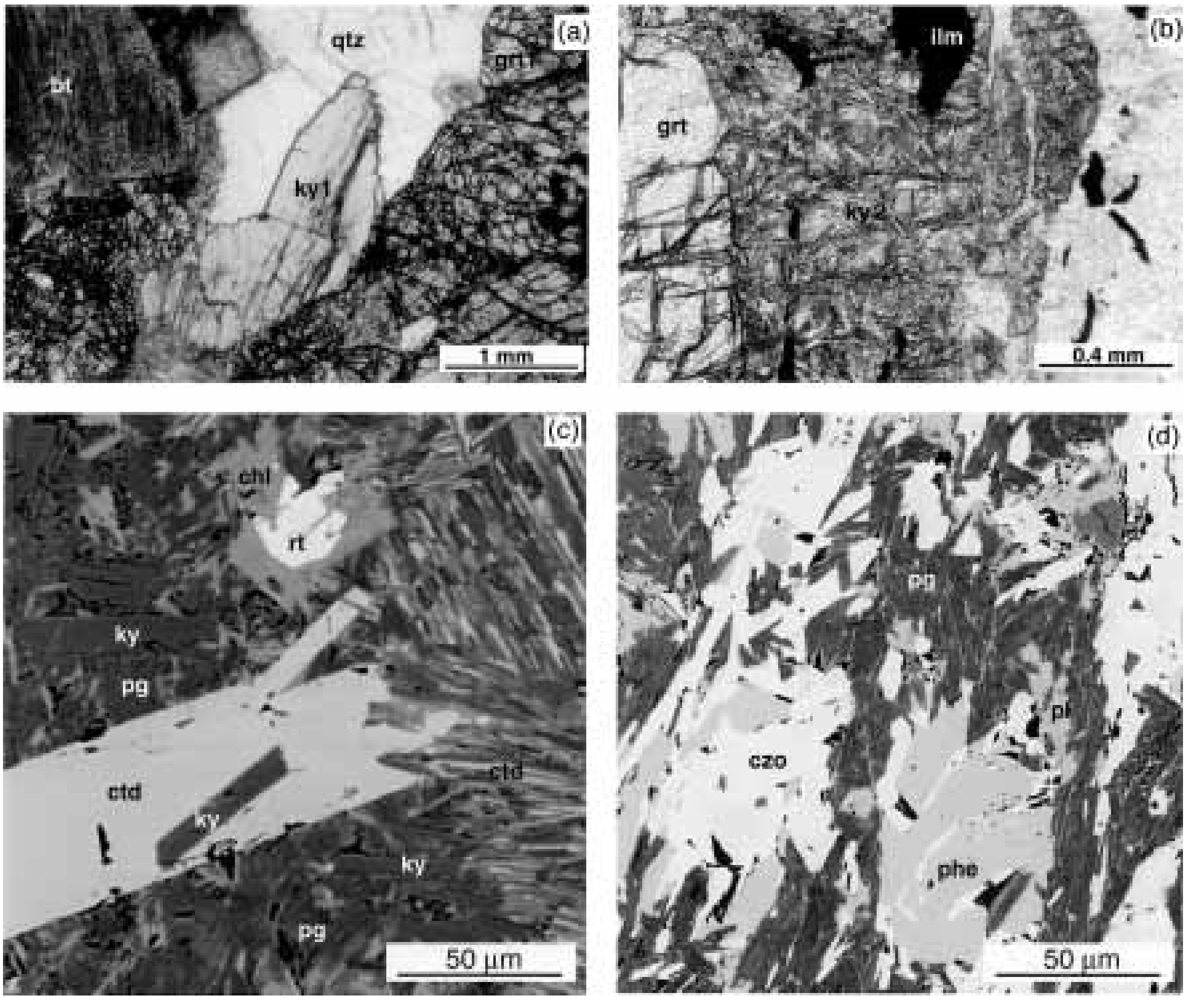


**Fig. 5.** Photomicrographs and BSE images of metapelite samples. (a) Granulite-facies paragenesis in metapelites. Large kyanite (ky1) coexists with garnet (grt1), biotite (bt) and quartz (qtz) in sample P-FS 108. (b) Kyanite has been replaced by fibrous kyanite (ky2) in sample G-FS 302. (c) Textural equilibrium among kyanite, chloritoid (ctd), and paragonite (pg) in sample G-FS 208. (d) Decomposition of plagioclase (pl) to paragonite, clinozoisite (czo) and phengite (phe) in sample G-FS 207.

clinopyroxene (Fig. 7). Garnet that appears to coexist with amphibole is richest in almandine content (Fig. 7). The Ca/Mg ratio of that garnet varies according to its predecessor pyroxene.

Apart from a variation in *mg*-number of amphibole related to bulk-rock chemistry, there is an overall trend of decreasing Al and alkali content (Fig. 8) within a single sample from garnet + amphibole coronas to biotite + amphibole coronas to amphibole pseudomorphs of pyroxene. The microstructural site strongly controls the chemical composition of pseudomorphic amphibole. Amphibole that has replaced clinopyroxene displays $TiO_2$ and $Al_2O_3$ contents similar to those of its predecessor (Table 4). In contrast, amphibole that has replaced orthopyroxene displays low $TiO_2$ and $Al_2O_3$ contents, and that which has overgrown olivine is an almost Al-free tremolite. Most analyzed amphibole and biotite grains contain significant amounts of Cl, which is highest in the texturally earliest corona amphibole of only weakly retrogressed granulites (Table 4). Amphibole and biotite in completely hydrated metagabbros show much lower Cl contents.

The composition of pre-Alpine amphibole differs clearly from amphibole formed during Alpine metamorphism (Fig. 8). Some tremolite that has replaced olivine shows prograde zoning towards barroisitic hornblende, which is typical of peak Alpine metamorphism (Guntli & Liniger, 1989). This provides evidence that the corona amphibole formed during pre-Alpine hydration of the gabbros.

*Table 4: Representative analyses of minerals from the Braccia gabbro*

| | Granular granulite | | | | | | | | Spinel–two-pyroxene corona | | | | | | Garnet–two-pyroxene corona | | | | | | |
|---|---|---|---|---|---|---|---|---|---|---|---|---|---|---|---|---|---|---|---|---|---|
| Sample: | B-F 7 | | | | | L-F 107 | | | B-F 7 | | | L-F 107 | | | B-F 7 | | | | L-F 107 | | |
| | $Cpx_1$ (core) | $Opx_1$ (core) | $Spl_1$ (core) | Ol (core) | Pl (core) | $Opx_1$ (core) | Ol (core) | Pl | $Cpx_2$ | $Opx_2$ | $Spl_2$ | $Cpx_2$ | $Opx_2$ | $Spl_2$ | $Cpx_3$ | $Opx_3$ | $Grt_1$ | $Grt_2$ | $Cpx_3$ | $Opx_3$ | $Grt_2$ |
| *wt %* | | | | | | | | | | | | | | | | | | | | | |
| $SiO_2$ | 48·9 | 52·4 | <0·06 | 37·2 | 54·7 | 52·4 | 38·4 | 53·6 | 50·5 | 52·2 | <0·06 | 50·86 | 52·8 | <0·06 | 52·1 | 55·5 | 38·2 | 37·9 | 51·2 | 54·1 | 39·9 |
| $TiO_2$ | 1·39 | 0·18 | <0·02 | <0·02 | <0·02 | 0·26 | <0·02 | <0·02 | 0·24 | <0·02 | <0·02 | 0·29 | 0·13 | 0·02 | 0·16 | 0·00 | <0·02 | 0·03 | 0·19 | 0·05 | 0·03 |
| $Cr_2O_3$ | 0·12 | 0·04 | 1·01 | <0·03 | <0·03 | 0·04 | <0·03 | <0·03 | 0·00 | <0·03 | <0·03 | <0·03 | <0·03 | 0·14 | <0·03 | 0·00 | <0·03 | 0·00 | <0·03 | <0·02 | <0·03 |
| $Al_2O_3$ | 7·03 | 4·90 | 60·6 | <0·03 | 28·6 | 4·66 | <0·03 | 29·5 | 4·08 | 3·87 | 63·3 | 5·00 | 4·29 | 65·0 | 2·72 | 1·01 | 22·5 | 22·1 | 3·28 | 2·48 | 22·4 |
| $Fe_2O_3$ | — | — | 2·13 | — | 0·44 | | — | 0·13 | — | — | 0·93 | — | — | 0·52 | — | — | 0·61 | 2·54 | — | — | 0·82 |
| FeO | 7·16 | 21·2 | 26·6 | 24·3 | — | 14·1 | 21·1 | — | 6·73 | 19·5 | 23·3 | 5·20 | 14·1 | 19·1 | 6·61 | 19·4 | 22·9 | 22·6 | 4·84 | 14·1 | 23·3 |
| NiO | 0·06 | <0·04 | 0·10 | 0·08 | <0·04 | — | 0·08 | — | 0·04 | 0·04 | 0·04 | 0·03 | 0·07 | 0·17 | 0·06 | <0·02 | <0·02 | <0·02 | <0·02 | — | — |
| MnO | 0·17 | 0·35 | 0·09 | 0·28 | <0·04 | 0·30 | 0·26 | <0·04 | 0·13 | 0·35 | 0·07 | 0·19 | 0·32 | 0·14 | 0·13 | 0·37 | 1·06 | 0·75 | 0·15 | 0·29 | 1·35 |
| MgO | 12·6 | 23·2 | 9·60 | 38·1 | 0·08 | 27·5 | 40·2 | <0·02 | 14·3 | 24·4 | 12·1 | 14·8 | 28·1 | 14·9 | 14·9 | 26·2 | 3·90 | 7·90 | 15·4 | 29·0 | 7·89 |
| CaO | 21·9 | 0·43 | <0·02 | <0·02 | 10·7 | 0·73 | <0·02 | 11·6 | 23·2 | 0·32 | <0·02 | 22·7 | 0·48 | <0·02 | 23·3 | 0·37 | 11·4 | 6·08 | 23·3 | 0·19 | 6·95 |
| $Na_2O$ | 1·44 | <0·03 | <0·03 | <0·03 | 5·63 | 0·03 | <0·03 | 5·07 | 0·66 | <0·03 | <0·03 | 0·98 | 0·03 | <0·03 | 0·58 | 0·02 | <0·03 | <0·03 | 0·78 | 0·03 | <0·03 |
| $K_2O$ | <0·03 | <0·03 | <0·03 | <0·03 | 0·03 | <0·03 | <0·03 | 0·02 | <0·03 | <0·03 | <0·03 | 0·03 | <0·02 | <0·03 | <0·03 | <0·03 | <0·03 | <0·03 | <0·03 | <0·03 | <0·03 |
| Σ | 100·6 | 102·9 | 100·3 | 100·1 | 100·2 | 99·9 | 100·0 | 99·9 | 99·9 | 100·7 | 99·9 | 100·0 | 100·3 | 100·1 | 100·5 | 102·8 | 100·6 | 100·0 | 99·1 | 100·3 | 102·7 |
| Si | 1·79 | 1·88 | 0·00 | 0·97 | 2·46 | 1·88 | 0·99 | 2·42 | 1·86 | 1·89 | 0·00 | 1·85 | 1·88 | 0·00 | 1·90 | 1·97 | 2·96 | 2·92 | 1·88 | 1·93 | 2·99 |
| Ti | 0·04 | 0·01 | 0·00 | 0·00 | 0·00 | 0·01 | 0·00 | 0·00 | 0·01 | 0·00 | 0·00 | 0·01 | 0·00 | 0·00 | 0·00 | 0·00 | 0·00 | 0·00 | 0·01 | 0·00 | 0·00 |
| Cr | 0·00 | 0·00 | 0·02 | 0·00 | 0·00 | 0·00 | 0·00 | 0·00 | 0·00 | 0·00 | 0·00 | 0·00 | 0·00 | 0·00 | 0·00 | 0·00 | 0·00 | 0·00 | 0·00 | 0·00 | 0·00 |
| Al | 0·30 | 0·21 | 1·94 | 0·00 | 1·51 | 0·20 | 0·00 | 0·00 | 0·18 | 0·17 | 1·98 | 0·22 | 0·18 | 1·99 | 0·12 | 0·04 | 2·05 | 2·01 | 0·14 | 0·10 | 1·98 |
| $Fe^{3+}$ | 0·00 | 0·00 | 0·04 | 0·00 | 0·01 | 0·00 | 0·00 | 0·01 | 0·00 | 0·00 | 0·02 | 0·00 | 0·00 | 0·01 | 0·00 | 0·00 | 0·04 | 0·15 | 0·00 | 0·00 | 0·05 |
| $Fe^{2+}$ | 0·22 | 0·63 | 0·60 | 0·53 | 0·00 | 0·42 | 0·46 | 0·00 | 0·21 | 0·59 | 0·52 | 0·16 | 0·42 | 0·41 | 0·20 | 0·58 | 1·48 | 1·45 | 0·15 | 0·42 | 1·46 |
| Ni | 0·00 | 0·00 | 0·00 | 0·00 | 0·00 | 0·00 | 0·00 | 0·00 | 0·00 | 0·00 | 0·00 | 0·00 | 0·00 | 0·01 | 0·00 | 0·00 | 0·00 | 0·00 | 0·00 | 0·00 | 0·00 |
| Mn | 0·01 | 0·01 | 0·00 | 0·01 | 0·00 | 0·01 | 0·01 | 0·00 | 0·00 | 0·01 | 0·00 | 0·01 | 0·01 | 0·00 | 0·00 | 0·01 | 0·07 | 0·05 | 0·01 | 0·01 | 0·09 |
| Mg | 0·69 | 1·25 | 0·39 | 1·49 | 0·01 | 1·47 | 1·55 | 0·00 | 0·78 | 1·32 | 0·48 | 0·80 | 1·49 | 0·58 | 0·81 | 1·39 | 0·45 | 0·91 | 0·84 | 1·54 | 0·88 |
| Ca | 0·86 | 0·02 | 0·00 | 0·00 | 0·52 | 0·03 | 0·00 | 0·56 | 0·92 | 0·01 | 0·00 | 0·89 | 0·02 | 0·00 | 0·91 | 0·01 | 0·95 | 0·50 | 0·92 | 0·01 | 0·56 |
| Na | 0·08 | 0·00 | 0·00 | 0·00 | 0·49 | 0·00 | 0·00 | 0·44 | 0·05 | 0·00 | 0·00 | 0·07 | 0·00 | 0·00 | 0·04 | 0·00 | 0·00 | 0·00 | 0·06 | 0·00 | 0·00 |
| K | 0·00 | 0·00 | 0·00 | 0·00 | 0·00 | 0·00 | 0·00 | 0·00 | 0·00 | 0·00 | 0·00 | 0·00 | 0·00 | 0·00 | 0·00 | 0·00 | 0·00 | 0·00 | 0·00 | 0·00 | 0·00 |
| *mg*-no. | 0·76 | 0·66 | 0·39 | 0·73 | | 0·78 | 0·77 | | 0·79 | 0·69 | 0·48 | 0·84 | 0·78 | 0·58 | 0·80 | 0·71 | 0·23 | 0·36 | 0·85 | 0·79 | 0·38 |

*Table 4: continued*

| | Garnet–amphibole corona | | | | | Biotite–garnet–amphibole corona | | | | | Biotite–amphibole corona | | | Pseudomorphic amphibole | |
|---|---|---|---|---|---|---|---|---|---|---|---|---|---|---|---|
| Sample: | B-F 7 | | L-F 107 | | G-F 105 | B-F 219 | | | | | B-F 110 | | | B-F 110 | |
| | $Grt_3$ | $Am_1$ | $Grt_3$ | $Am_1$ | $Am_1$ | $Grt_4$ | $Am_2$ | Bt | Ilm | Pl | $Am_2$ | Bt | Pl | $Am_3$ | $Am_4$ |
| *wt %* | | | | | | | | | | | | | | | |
| $SiO_2$ | 37·4 | 41·5 | 37·7 | 39·8 | 39·7 | 37·6 | 43·6 | 38·6 | <0·06 | 59·5 | 43·9 | 38·9 | 57·1 | 42·8 | 51·2 |
| $TiO_2$ | 0·03 | <0·02 | 0·02 | 0·03 | 0·02 | 0·06 | 0·44 | 1·27 | 52·3 | <0·02 | 0·18 | 1·65 | <0·02 | 0·26 | 0·63 |
| $Cr_2O_3$ | <0·03 | <0·03 | <0·03 | <0·03 | <0·03 | <0·03 | <0·03 | 0·03 | <0·03 | <0·03 | 0·02 | 0·06 | <0·03 | <0·03 | 0·10 |
| $Al_2O_3$ | 21·9 | 19·3 | 22·0 | 20·7 | 20·0 | 21·7 | 15·2 | 17·5 | <0·03 | 26·5 | 12·9 | 15·8 | 27·3 | 14·6 | 6·24 |
| $Fe_2O_3$ | 1·55 | 4·50 | 1·04 | 4·00 | 4·45 | 1·13 | 4·95 | — | 1·71 | 0·08 | 4·37 | — | 0·10 | 3·72 | 4·49 |
| FeO | 26·0 | 9·45 | 26·2 | 8·40 | 14·4 | 30·9 | 10·4 | 12·5 | 45·1 | — | 12·9 | 16·8 | — | 13·1 | 9·42 |
| MnO | 0·79 | 0·08 | 0·56 | 0·13 | 0·23 | 1·76 | 0·12 | 0·04 | 0·34 | <0·02 | 0·20 | 0·06 | 0·04 | 0·22 | 0·13 |
| MgO | 3·39 | 9·83 | 3·84 | 10·9 | 5·99 | 4·02 | 10·4 | 17·4 | 0·80 | <0·02 | 9·89 | 13·4 | <0·02 | 8·90 | 14·5 |
| CaO | 9·21 | 9·97 | 8·88 | 9·56 | 11·8 | 4·53 | 10·4 | 0·08 | <0·02 | 7·25 | 12·2 | 0·49 | 9·29 | 11·8 | 12·1 |
| $Na_2O$ | <0·03 | 3·12 | <0·03 | 3·47 | 1·55 | <0·03 | 2·47 | 0·65 | <0·03 | 7·47 | 1·30 | 0·45 | 6·52 | 1·33 | 0·7 |
| $K_2O$ | <0·03 | 0·65 | <0·03 | 0·53 | 0·32 | <0·03 | 0·58 | 7·80 | <0·03 | 0·30 | 0·52 | 8·46 | 0·04 | 0·50 | 0·13 |
| Cl | <0·03 | 0·06 | <0·03 | 0·26 | 0·63 | — | — | — | — | — | 0·18 | 0·22 | <0·03 | 0·17 | 0·08 |
| $H_2O$ | | 2·05 | | 2·00 | 1·87 | | 2·07 | 4·14 | | | | 3·98 | | 2·04 | 2·08 |
| Σ | 100·2 | 100·6 | 100·3 | 99·7 | 100·8 | 100·9 | 100·7 | 100·0 | 100·4 | 101·2 | 100·5 | 100·3 | 100·4 | 99·4 | 101·8 |
| Si | 2·94 | 6·00 | 2·95 | 5·80 | 5·88 | 2·96 | 6·33 | 2·80 | 0·00 | 2·62 | 6·47 | 2·90 | 2·55 | 6·36 | 7·23 |
| Ti | 0·00 | 0·00 | 0·00 | 0·00 | 0·00 | 0·00 | 0·05 | 0·07 | 0·98 | 0·00 | 0·02 | 0·09 | 0·00 | 0·03 | 0·07 |
| Cr | 0·00 | 0·00 | 0·00 | 0·00 | 0·00 | 0·00 | 0·00 | 0·00 | 0·00 | 0·00 | 0·00 | 0·00 | 0·00 | 0·00 | 0·01 |
| Al | 2·03 | 3·29 | 2·03 | 3·54 | 3·48 | 2·01 | 2·60 | 1·50 | 0·00 | 1·38 | 2·24 | 1·38 | 1·43 | 2·56 | 1·04 |
| $Fe^{3+}$ | 0·09 | 0·49 | 0·06 | 0·44 | 0·50 | 0·07 | 0·54 | 0·00 | 0·03 | 0·00 | 0·48 | 0·00 | 0·00 | 0·42 | 0·48 |
| $Fe^{2+}$ | 1·71 | 1·14 | 1·72 | 1·02 | 1·78 | 1·98 | 1·26 | 0·76 | 0·95 | 0·00 | 1·59 | 1·05 | 0·00 | 1·62 | 1·11 |
| Mn | 0·05 | 0·01 | 0·04 | 0·02 | 0·03 | 0·12 | 0·02 | 0·00 | 0·01 | 0·00 | 0·03 | 0·00 | 0·00 | 0·03 | 0·02 |
| Mg | 0·40 | 2·12 | 0·45 | 2·36 | 1·32 | 0·47 | 2·25 | 1·88 | 0·03 | 0·00 | 2·17 | 1·48 | 0·00 | 1·97 | 3·05 |
| Ca | 0·78 | 1·55 | 0·75 | 1·49 | 1·87 | 0·38 | 1·61 | 0·01 | 0·00 | 0·34 | 1·92 | 0·04 | 0·44 | 1·88 | 1·83 |
| Na | 0·00 | 0·87 | 0·00 | 0·98 | 0·45 | 0·00 | 0·69 | 0·09 | 0·00 | 0·64 | 0·37 | 0·06 | 0·56 | 0·38 | 0·19 |
| K | 0·00 | 0·12 | 0·00 | 0·10 | 0·06 | 0·00 | 0·11 | 0·72 | 0·00 | 0·02 | 0·10 | 0·80 | 0·00 | 0·09 | 0·02 |
| Cl | 0·00 | 0·02 | 0·00 | 0·06 | 0·16 | | | | | | 0·04 | 0·03 | | 0·04 | 0·02 |
| OH | | 1·98 | | 1·94 | 1·84 | | 2·00 | 2·00 | | | 1·96 | 1·97 | | 1·96 | 1·98 |
| *mg*-no. | 0·18 | 0·57 | 0·20 | 0·62 | 0·37 | 0·19 | 0·56 | 0·71 | 0·96 | | 0·51 | 0·59 | | 0·49 | 0·68 |

Single representative point analyses of mineral grains are given. Unless stated otherwise, analyses from contacting grains in coronas are given. Analytical conditions: wavelength-dispersive spectrometers on a Cameca SX 50 electron microprobe: 15 kV acceleration voltage, 20 nA beam current; beam size of 1 μm, 20 s counting time on peak and half that time on background position on either side of the peak, 10 s for Na and K, 40 s for Cl. A ZAF-type correction procedure was applied to the data (Pouchou & Pichoir, 1984). Normalization of minerals was made by using the program NORM (written by P. Ulmer, ETH Zürich): pyroxene to six oxygens, olivine to three cations and four oxygens, plagioclase to five cations and eight oxygens, spinel to three cations and four oxygens, garnet to eight cations and 12 oxygens; amphibole was normalized to 23 oxygens and $Fe^{3+}/Fe^{tot} = 0·3$; biotite to 11 oxygens. Average relative error as listed in Table 5.

*Table 5: Representative analyses of minerals from the Malenco peridotite*

| | Granoblastic equilibration | | | | | | | | | | | | | | | Chlorite–amphibole coronas | | | | | |
|---|---|---|---|---|---|---|---|---|---|---|---|---|---|---|---|---|---|---|---|---|---|
| Sample: | L-UM 112 | | | | | L-UM 216 | | | | | L-UM 400 | | | | | L-UM 400 | | | L-UM 216 | | |
| | $Ol_2$ | $Cpx_2$ | $Opx_2$ | $Spl_2$ | Ti-prg | $Ol_2$ | $Cpx_2$ | $Opx_2$ | $Spl_2$ | Ti-prg | $Ol_2$ | $Cpx_2$ | $Opx_2$ | $Spl_2$ | Ti-prg | Cr-Spl | Chl | MgHbl | Cr-Spl | Chl | MgHbl |
| *wt %* | | | | | | | | | | | | | | | | | | | | | |
| $SiO_2$ | 41·0 | 54·6 | 57·2 | <0·02 | 43·3 | 40·7 | 54·6 | 57·1 | <0·02 | 43·2 | 41·7 | 54·5 | 56·7 | <0·02 | 44·5 | 0·33 | 31·2 | 53·36 | <0·10 | 32·0 | 55·2 |
| $TiO_2$ | <0·02 | 0·21 | 0·07 | 0·03 | 2·00 | <0·02 | 0·34 | <0·02 | <0·02 | 3·11 | <0·02 | 0·19 | 0·05 | 0·23 | 1·76 | 0·30 | 0·05 | 0·21 | 0·21 | <0·02 | 0·15 |
| $Cr_2O_3$ | <0·03 | 0·22 | 0·34 | 19·3 | 1·27 | <0·03 | 0·24 | 0·23 | 13·3 | 1·02 | <0·03 | 0·50 | 0·40 | 14·4 | 2·09 | 60·8 | 1·56 | 1·42 | 61·7 | 0·17 | 0·38 |
| $Al_2O_3$ | <0·06 | 2·56 | 2·61 | 48·1 | 14·3 | <0·06 | 2·70 | 2·56 | 54·7 | 14·2 | <0·06 | 2·84 | 2·74 | 53·9 | 12·5 | 4·62 | 19·0 | 4·57 | 4·33 | 19·0 | 4·19 |
| $Fe_2O_3$* | | | | 1·82 | 0·87 | | | | 0·76 | 1·33 | | | | 0·11 | | 0·60 | | | 0·67 | — | |
| FeO | 10·8 | 2·01 | 5·80 | 14·8 | 2·34 | 10·1 | 2·11 | 7·35 | 12·9 | 2·78 | 9·40 | 2·16 | 5·64 | 12·6 | 3·16 | 26·3 | 2·17 | 1·64 | 26·6 | 2·42 | 2·01 |
| NiO | 0·41 | 0·05 | 0·08 | 0·21 | 0·15 | 0·36 | 0·06 | 0·06 | 0·42 | 0·20 | 0·39 | <0·02 | 0·08 | 0·26 | 0·08 | <0·02 | 0·25 | 0·04 | 0·20 | 0·30 | 0·10 |
| MnO | 0·16 | 0·08 | 0·16 | 0·31 | 0·06 | 0·13 | 0·06 | 0·11 | 0·13 | 0·08 | 0·13 | 0·10 | 0·17 | 0·18 | 0·07 | 0·75 | <0·02 | <0·02 | 0·78 | <0·02 | <0·02 |
| MgO | 48·1 | 17·5 | 34·7 | 16·0 | 17·5 | 48·8 | 17·4 | 33·6 | 17·9 | 17·5 | 50·2 | 16·0 | 34·6 | 18·1 | 17·8 | 3·58 | 31·6 | 22·7 | 3·18 | 32·9 | 23·5 |
| CaO | <0·02 | 23·5 | 0·32 | | 11·8 | <0·02 | 23·1 | 0·28 | <0·02 | 11·7 | <0·02 | 21·8 | 0·43 | | 12·3 | 0·11 | 0·05 | 12·7 | 0·06 | <0·02 | 12·8 |
| $Na_2O$ | | 0·92 | 0·03 | | 3·65 | na | 0·95 | 0·04 | na | 3·63 | | 1·49 | 0·05 | | 3·23 | | 0·22 | 1·89 | na | <0·03 | 1·69 |
| $K_2O$ | | <0·02 | | | 0·22 | na | <0·02 | <0·02 | na | 0·02 | | <0·02 | | | 0·12 | | 0·10 | 0·05 | na | <0·02 | <0·02 |
| Cl | | | | | <0·01 | | na | na | | <0·01 | | | | | 0·02 | | | 0·01 | na | <0·01 | 0·05 |
| $H_2O$ calc | | | | | 2·14 | | | | | 2·13 | | | | | 2·11 | | 12·69 | 2·17 | | 12·77 | 2·22 |
| $\Sigma$ | 100·4 | 101·6 | 101·3 | 100·5 | 99·6 | 100·1 | 101·5 | 101·2 | 100·1 | 100·9 | 101·8 | 101·3 | 100·8 | 99·9 | 99·7 | 97·4 | 98·9 | 100·7 | 97·7 | 99·6 | 102·2 |
| Si | 1·006 | 1·948 | 1·942 | 0·000 | 6·147 | 0·999 | 1·947 | 1·949 | 0·001 | 6·083 | 1·001 | 1·906 | 1·935 | 0·000 | 6·331 | 0·012 | 2·964 | 7·329 | 0·006 | 3·003 | 7·441 |
| Ti | 0·000 | 0·006 | 0·002 | 0·001 | 0·214 | 0·000 | 0·010 | 0·001 | 0·002 | 0·329 | 0·000 | 0·010 | 0·001 | 0·005 | 0·189 | 0·008 | 0·034 | 0·021 | 0·006 | 0·000 | 0·015 |
| Cr | 0·000 | 0·006 | 0·009 | 0·416 | 0·143 | 0·000 | 0·007 | 0·006 | 0·277 | 0·114 | 0·000 | 0·026 | 0·011 | 0·303 | 0·235 | 1·745 | 0·117 | 0·155 | 1·774 | 0·013 | 0·041 |
| Al | 0·000 | 0·108 | 0·105 | 1·545 | 2·393 | 0·000 | 0·114 | 0·103 | 1·703 | 2·346 | 0·000 | 0·216 | 0·111 | 1·685 | 2·086 | 0·198 | 2·063 | 0·740 | 0·186 | 2·099 | 0·666 |
| $Fe^{3+}$ | | | | 0·037 | 0·093 | | | | 0·015 | 0·140 | | | | 0·002 | | 0·017 | | | 0·018 | | |
| $Fe^{2+}$ | 0·221 | 0·060 | 0·165 | 0·337 | 0·278 | 0·207 | 0·063 | 0·210 | 0·285 | 0·328 | 0·189 | 0·065 | 0·161 | 0·280 | 0·376 | 0·799 | 0·173 | 0·188 | 0·810 | 0·190 | 0·227 |
| Ni | 0·008 | 0·001 | 0·002 | 0·005 | 0·018 | 0·007 | 0·001 | 0·001 | 0·009 | 0·011 | 0·008 | 0·000 | 0·002 | 0·006 | 0·009 | 0·000 | 0·018 | 0·005 | 0·002 | 0·023 | 0·008 |
| Mn | 0·003 | 0·002 | 0·005 | 0·007 | 0·008 | 0·003 | 0·002 | 0·003 | 0·003 | 0·010 | 0·001 | 0·003 | 0·005 | 0·004 | 0·009 | 0·023 | 0·004 | 0·002 | 0·024 | 0·004 | 0·000 |
| Mg | 1·761 | 0·929 | 1·752 | 0·650 | 3·707 | 1·784 | 0·926 | 1·710 | 0·706 | 3·661 | 1·799 | 0·851 | 1·760 | 0·715 | 3·765 | 0·194 | 4·475 | 4·646 | 0·173 | 4·606 | 4·722 |
| Ca | 0·000 | 0·898 | 0·012 | | 1·802 | 0·001 | 0·883 | 0·010 | 0·000 | 1·770 | 0·000 | 0·836 | 0·016 | | 1·877 | 0·004 | 0·005 | 1·861 | 0·018 | 0·000 | 1·848 |
| Na | | 0·063 | 0·002 | | 1·006 | | 0·066 | 0·004 | | 0·990 | | 0·103 | 0·003 | | 0·891 | | 0·041 | 0·505 | | 0·000 | 0·442 |
| K | | | | | 0·040 | | 0·000 | 0·000 | | 0·001 | | 0·000 | | | 0·021 | | 0·013 | 0·009 | | 0·000 | 0·004 |
| Cl | | | | | 0·000 | | | | | 0·000 | | | | | 0·005 | | | 0·003 | | 0·000 | 0·006 |
| OH | | | | | 2·000 | | | | | 2·000 | | | | | 1·995 | | 8·000 | 1·997 | | 8·000 | 1·994 |
| *mg*-no. | 0·884 | 0·939 | 0·914 | 0·650 | 0·909 | 0·891 | 0·936 | 0·891 | 0·703 | 0·887 | 0·900 | 0·929 | 0·916 | 0·708 | 0·909 | 0·188 | 0·963 | 0·961 | 0·170 | 0·960 | 0·954 |

*Table 5: continued*

| | Recrystallized matrix | | | | | | | | | | | | | Serp. mylonite | | | Oceanic stage | | |
|---|---|---|---|---|---|---|---|---|---|---|---|---|---|---|---|---|---|---|---|
| Sample: | L-UM 400 | | | L-UM 112 | | | Or-UM 224 | | | | | L-UM 226 | | Or-UM 224 | | | L-UM 226 | | |
| | $Ol_2$ | Tr | Chl | $Ol_2$ | Tr | Chl | $Ol_2$ | Tr | Chl | Cr-mag | Ilm | Tr | Tlc | Di | Atg | Chl | Chr | Chl | Av. rel. error ($2\sigma$) (%) |
| *wt %* | | | | | | | | | | | | | | | | | | | |
| $SiO_2$ | 41·2 | 59·0 | 34·5 | 40·7 | 57·0 | 34·6 | 40·3 | 57·3 | 34·2 | <0·06 | <0·06 | 57·3 | 61·5 | 55·3 | 43·3 | 34·4 | 35·4 | 36·0 | 0·6 (at 40% level) |
| $TiO_2$ | <0·02 | <0·02 | <0·02 | <0·02 | <0·02 | 0·04 | <0·02 | <0·10 | <0·02 | 3·09 | 52·1 | 0·06 | 0·04 | <0·02 | <0·02 | <0·02 | <0·02 | <0·02 | 6·2 (at 0·2% level) |
| $Cr_2O_3$ | <0·03 | <0·03 | 1·02 | <0·03 | 0·26 | 1·21 | <0·03 | 0·09 | 2·15 | 25·0 | 0·07 | 0·35 | 0·08 | 0·06 | 0·70 | 1·89 | <0·03 | 2·08 | 3·8 (at 0·6% level) |
| $Al_2O_3$ | <0·06 | 0·45 | 13·0 | <0·06 | 0·74 | 12·2 | <0·06 | 1·20 | 12·6 | 0·17 | <0·06 | 1·07 | 0·37 | 0·32 | 3·04 | 12·5 | <0·06 | 10·5 | 1·2 (at 10% level) |
| $Fe_2O_3$* | | | | | | | | | | 37·3 | 1·91 | | | | — | — | | — | |
| FeO | 9·91 | 1·61 | 3·78 | 11·7 | 1·51 | 3·32 | 13·29 | 2·06 | 3·70 | 31·1 | 40·0 | 2·43 | 1·27 | 1·72 | 4·30 | 3·54 | 7·53 | 4·43 | 2·8 (at 10% level) |
| NiO | 0·49 | 0·14 | 0·22 | 0·35 | 0·04 | 0·21 | 0·35 | 0·08 | 0·26 | 0·54 | 0·10 | 0·12 | 0·20 | 0·06 | 0·15 | 0·25 | 0·35 | 0·25 | 8·0 (at 0·4% level) |
| MnO | 0·13 | 0·03 | <0·02 | 0·19 | 0·05 | <0·02 | 0·24 | 0·04 | <0·02 | 0·09 | 1·47 | 0·06 | 0·04 | 0·12 | <0·02 | <0·02 | 0·10 | <0·02 | 20·4 (at 0·2% level) |
| MgO | 50·0 | 24·4 | 34·4 | 47·4 | 24·1 | 35·1 | 46·6 | 23·9 | 34·4 | 0·89 | 2·70 | 24·1 | 31·3 | 18·1 | 37·6 | 34·5 | 40·2 | 34·3 | 1·0 (at 20% level) |
| CaO | <0·02 | 12·6 | 0·06 | 0·03 | 12·9 | 0·07 | <0·02 | 12·0 | <0·02 | 0·10 | 0·27 | 11·6 | 0·06 | 25·4 | <0·02 | <0·02 | <0·02 | 0·09 | 1·2 (at 10% level) |
| $Na_2O$ | | 0·37 | | | 0·63 | <0·03 | | 2·47 | <0·03 | | <0·03 | 1·09 | 0·18 | 0·26 | <0·03 | <0·03 | <0·03 | <0·03 | 4·2 (at 1% level) |
| $K_2O$ | | 0·03 | | | 0·02 | <0·03 | | 0·13 | <0·03 | | <0·02 | 0·06 | <0·02 | <0·02 | <0·02 | <0·02 | <0·02 | <0·02 | 10·0 (at 0·2% level) |
| Cl | | 0·02 | | | 0·01 | | | 0·04 | — | | | | <0·01 | | 0·01 | 0·02 | 0·06 | 0·02 | 7·2 (at 0·05% level) |
| $H_2O$ calc | | 2·21 | 12·67 | | 2·18 | 12·64 | | 2·21 | 12·66 | | | 2·20 | 4·69 | | 12·24 | 12·69 | 11·77 | 12·71 | |
| $\Sigma$ | 101·8 | 100·8 | 99·7 | 100·5 | 99·5 | 99·4 | 100·8 | 101·3 | 100·0 | 98·3 | 98·5 | 100·4 | 99·7 | 101·2 | 101·2 | 99·8 | 95·4 | 100·5 | |
| Si | 0·994 | 7·939 | 3·267 | 1·004 | 7·835 | 3·280 | 0·996 | 7·766 | 3·237 | 0·001 | 0·002 | 7·819 | 3·934 | 1·983 | 32·92 | 3·256 | 3·605 | 3·401 | |
| Ti | 0·000 | 0·001 | 0·001 | 0·000 | 0·000 | 0·003 | 0·000 | 0·004 | 0·002 | 0·089 | 0·980 | 0·003 | 0·002 | 0·000 | 0·00 | 0·000 | 0·000 | 0·003 | |
| Cr | 0·000 | 0·003 | 0·076 | 0·000 | 0·028 | 0·091 | 0·000 | 0·010 | 0·161 | 0·754 | 0·001 | 0·038 | 0·004 | 0·002 | 0·42 | 0·141 | 0·000 | 0·155 | |
| Al | 0·000 | 0·072 | 1·446 | 0·000 | 0·119 | 1·363 | 0·000 | 0·191 | 1·404 | 0·008 | 0·000 | 0·173 | 0·028 | 0·013 | 2·72 | 1·399 | 0·001 | 1·173 | |
| $Fe^{3+}$ | | | | | | | | | | 1·071 | 0·036 | | | | | | | | |
| $Fe^{2+}$ | 0·220 | 0·181 | 0·299 | 0·242 | 0·174 | 0·264 | 0·275 | 0·233 | 0·293 | 0·993 | 0·838 | 0·277 | 0·068 | 0·052 | 2·73 | 0·280 | 0·642 | 0·350 | |
| Ni | 0·010 | 0·015 | 0·016 | 0·007 | 0·005 | 0·016 | 0·007 | 0·010 | 0·020 | 0·011 | 0·002 | 0·014 | 0·010 | 0·001 | 0·09 | 0·182 | 0·028 | 0·015 | |
| Mn | 0·003 | 0·003 | 0·000 | 0·004 | 0·005 | 0·000 | 0·005 | 0·002 | 0·000 | 0·003 | 0·031 | 0·006 | 0·003 | 0·004 | 0·03 | 0·000 | 0·001 | 0·000 | |
| Mg | 1·793 | 4·887 | 4·856 | 1·741 | 4·933 | 4·959 | 1·716 | 4·830 | 4·853 | 0·051 | 0·101 | 4·897 | 2·985 | 0·966 | 42·59 | 4·868 | 6·103 | 4·821 | |
| Ca | 0·000 | 1·861 | 0·006 | 0·000 | 1·906 | 0·007 | 0·001 | 1·747 | 0·004 | 0·004 | 0·071 | 1·698 | 0·005 | 0·977 | 0·01 | 0·008 | 0·003 | 0·001 | |
| Na | | 0·098 | | | 0·169 | | | 0·649 | | | 0·001 | 0·287 | 0·022 | 0·018 | 0·00 | 0·001 | 0·001 | 0·001 | |
| K | | 0·005 | | | 0·003 | | | 0·022 | | | 0·001 | 0·010 | 0·001 | 0·000 | 0·00 | 0·001 | 0·001 | 0·002 | |
| Cl | | 0·001 | | | 0·001 | | | 0·003 | | | | 0·000 | 0·000 | | 0·00 | 0·000 | 0·018 | 0·000 | |
| OH | | 1·999 | 2·000 | | 1·999 | 8·000 | | 1·997 | 2·000 | | | 2·000 | 2·000 | | 62·00 | 2·000 | 7·982 | 8·000 | |
| *mg*-no. | 0·894 | 0·964 | 0·942 | 0·872 | 0·969 | 0·949 | 0·856 | 0·954 | 0·943 | 0·044 | 0·103 | 0·946 | 0·978 | 0·953 | 0·940 | 0·946 | 0·905 | 0·932 | |

Single representative point analyses of neighboring mineral grains are given. Analytical conditions as in Table 4, except counting time for Ni (40 s). Ions calculated on the basis of three cations (olivine), three cations and four oxygens (spinel), six oxygens (pyroxenes), $\Sigma$(cations) − Na − K − Ca = 13 (amphiboles), 14 oxygens (chlorite, serpentine), two cations (ilmenite), 147 oxygens (antigorite) and 11 oxygens (talc).
*Calculated assuming stoichiometry.

*Table 6: Representative analyses of minerals from pelitic granulite*

| | Granulite facies | | | | | | Granulite stage II | | | | | Hydrous recrystallization (amphibolite facies) | | | | | | | | | |
|---|---|---|---|---|---|---|---|---|---|---|---|---|---|---|---|---|---|---|---|---|---|
| Sample: | G-FS 205 | | | G-FS 207 | | | G-FS 207 | | G-FS 205 small grain | | | G-FS 207 | | G-FS 205 | | | G-FS 208 | | | | |
| | core $Grt_1$ | rim1 $Grt_2$ | rim2 $Grt_3$ | $Grt_1$* | ilm* | Pl* | $Grt_2$* | Bt* | $Grt_3$* | $Grt_4$* | Pl* | St* | Ctd* | Czo | Pg* | Phe | Ctd | Czo | Pg | Phe | Av. rel. error (2σ) (%) |
| *wt %* | | | | | | | | | | | | | | | | | | | | | |
| $SiO_2$ | 38·4 | 37·4 | 36·9 | 39·2 | <0·06 | 57·3 | 38·0 | 34·6 | 37·9 | 37·7 | 56·1 | 28·6 | 25·2 | 39·7 | 50·2 | 51·7 | 24·4 | 40·4 | 48·8 | 50·7 | 0·6 (at 40% level) |
| $TiO_2$ | 0·07 | 0·04 | <0·02 | 0·04 | 52·8 | <0·02 | 0·06 | 1·15 | <0·02 | <0·02 | <0·02 | <0·02 | <0·02 | 0·05 | 0·07 | 0·41 | <0·02 | 0·04 | 0·04 | 0·27 | 6·2 (at 0·2% level) |
| $Cr_2O_3$ | — | — | — | 0·10 | 0·05 | <0·03 | 0·09 | 0·07 | — | — | — | <0·03 | 0·19 | — | — | — | — | — | — | — | 4·6 (at 0·1% level) |
| $Al_2O_3$ | 21·7 | 21·5 | 21·2 | 22·1 | <0·03 | 27·7 | 21·1 | 20·8 | 21·8 | 21·6 | 26·9 | 55·1 | 42·1 | 32·1 | 39·4 | 30·3 | 41·1 | 32·7 | 40·1 | 32·0 | 1·0 (at 20% level) |
| $Fe_2O_3$† | 1·83 | 1·83 | 2·26 | 0·96 | — | 0·08 | 0·29 | — | 0·89 | 1·71 | <0·02 | — | 0·08 | 2·05 | 0·26 | 1·80 | 0·41 | 0·85 | 0·10 | 0·89 | |
| FeO | 26·3 | 30·3 | 29·1 | 26·1 | 45·7 | — | 30·6 | 14·9 | 33·3 | 26·0 | — | 12·0 | 16·4 | — | — | — | 23·8 | — | — | — | 2·8 (at 10% level) |
| MnO | 1·10 | 0·96 | 0·81 | 0·99 | 0·41 | <0·04 | 1·49 | 0·04 | 0·45 | 0·78 | <0·04 | 0·10 | 0·05 | 0·04 | <0·04 | 0·06 | 0·37 | 0·05 | <0·04 | <0·04 | 20·4 (at 0·2% level) |
| MgO | 9·30 | 6·45 | 1·92 | 9·68 | 0·52 | <0·02 | 5·97 | 12·8 | 2·60 | 3·26 | <0·02 | 2·12 | 7·61 | <0·02 | 0·08 | 2·88 | 2·82 | 0·04 | 0·06 | 2·26 | 1·2 (at 10% level) |
| CaO | 1·57 | 1·52 | 8·32 | 1·84 | <0·02 | 9·22 | 2·06 | 0·07 | 5·37 | 9·64 | 9·34 | 0·02 | <0·02 | 24·3 | 0·27 | <0·02 | <0·02 | 24·1 | 0·78 | <0·02 | 1·2 (at 10% level) |
| $Na_2O$ | <0·03 | <0·03 | <0·03 | <0·03 | <0·03 | 6·65 | <0·03 | 0·18 | <0·03 | <0·03 | 6·38 | <0·03 | <0·03 | <0·03 | 6·33 | 0·66 | <0·03 | <0·03 | 5·80 | 0·66 | 4·2 (at 1% level) |
| $K_2O$ | <0·03 | <0·03 | <0·03 | <0·03 | <0·03 | 0·05 | <0·03 | 9·36 | <0·03 | <0·03 | 0·04 | <0·03 | <0·03 | <0·03 | 0·83 | 9·60 | <0·03 | <0·03 | 1·12 | 9·75 | 10·0 (at 0·2% level) |
| $H_2O$ calc | | | | | | | | 3·96 | | | | 2·19 | 7·51 | 1·97 | 4·85 | 4·67 | 7·32 | 1·98 | 4·82 | 4·63 | |
| Σ | 100·3 | 100·1 | 100·4 | 101·0 | 99·5 | 101·0 | 100·1 | 98·0 | 102·4 | 100·8 | 98·9 | 100·2 | 99·2 | 100·2 | 102·3 | 102·1 | 100·4 | 100·1 | 100·8 | 101·2 | |
| Si | 2·96 | 2·95 | 2·94 | 2·98 | 0·00 | 2·54 | 2·99 | 2·62 | 2·97 | 2·95 | 2·54 | 7·82 | 2·01 | 3·02 | 3·01 | 3·32 | 2·00 | 3·05 | 3·04 | 3·28 | |
| Ti | 0·00 | 0·00 | 0·00 | 0·00 | 1·00 | 0·00 | 0·00 | 0·07 | 0·00 | 0·00 | 0·00 | 0·01 | 0·00 | 0·00 | 0·00 | 0·02 | 0·00 | 0·00 | 0·00 | 0·00 | |
| Cr | 0·00 | 0·00 | 0·00 | 0·01 | 0·00 | 0·00 | 0·01 | 0·00 | 0·00 | 0·00 | 0·00 | 0·00 | 0·01 | 0·00 | 0·00 | 0·00 | 0·00 | 0·00 | 0·00 | 0·00 | |
| Al | 1·97 | 2·00 | 1·99 | 1·98 | 0·00 | 1·45 | 1·99 | 1·85 | 2·01 | 2·00 | 1·44 | 17·80 | 3·96 | 2·87 | 2·87 | 2·30 | 3·97 | 2·91 | 2·95 | 2·44 | |
| $Fe^{3+}$ | 0·11 | 0·11 | 0·14 | 0·06 | 0·00 | 0·00 | 0·02 | 0·00 | 0·05 | 0·10 | 0·00 | 0·00 | 0·01 | 0·12 | 0·01 | 0·09 | 0·03 | 0·05 | 0·01 | 0·04 | |
| $Fe^{2+}$ | 1·69 | 1·99 | 1·94 | 1·66 | 0·97 | 0·00 | 2·01 | 0·95 | 2·18 | 1·70 | 0·00 | 2·74 | 1·10 | 0·00 | 0·00 | 0·00 | 1·63 | 0·00 | 0·00 | 0·00 | |
| Mn | 0·07 | 0·06 | 0·06 | 0·06 | 0·01 | 0·00 | 0·10 | 0·00 | 0·03 | 0·05 | 0·00 | 0·02 | 0·00 | 0·00 | 0·00 | 0·00 | 0·03 | 0·00 | 0·00 | 0·00 | |
| Mg | 1·07 | 0·76 | 0·23 | 1·10 | 0·02 | 0·00 | 0·70 | 1·45 | 0·30 | 0·38 | 0·00 | 0·87 | 0·91 | 0·00 | 0·01 | 0·28 | 0·34 | 0·00 | 0·00 | 0·22 | |
| Ca | 0·13 | 0·13 | 0·71 | 0·15 | 0·00 | 0·44 | 0·17 | 0·01 | 0·45 | 0·81 | 0·45 | 0·01 | 0·00 | 1·98 | 0·02 | 0·00 | 0·00 | 1·95 | 0·01 | 0·00 | |
| Na | 0·00 | 0·00 | 0·00 | 0·00 | 0·00 | 0·57 | 0·00 | 0·03 | 0·00 | 0·00 | 0·56 | 0·00 | 0·00 | 0·00 | 0·76 | 0·08 | 0·00 | 0·00 | 0·70 | 0·08 | |
| K | 0·00 | 0·00 | 0·00 | 0·00 | 0·00 | 0·00 | 0·00 | 0·90 | 0·00 | 0·00 | 0·00 | 0·00 | 0·00 | 0·00 | 0·07 | 0·79 | 0·00 | 0·00 | 0·09 | 0·81 | |
| H | | | | | | | | 2·00 | | | | 4·00 | 4·00 | 1·00 | 2·00 | 2·00 | 4·00 | 1·00 | 2·00 | 2·00 | |
| *X*Mg | 0·37 | 0·27 | 0·10 | 0·37 | 0·02 | | 0·25 | 0·61 | 0·12 | 0·17 | | 0·24 | 0·45 | | | | 0·17 | | | | |

*From Hermann *et al.* (1997)
†Calculated assuming stoichiometry.
Single representative point analyses of mineral grains are given. Analytical conditions as in Table 4. Cations are calculated on the basis of eight cations, 12 oxygens (Grt); two cations, three oxygens (Ilm); five cations, eight oxygens (Pl); 46 oxygens (St); eight cations, 12 oxygens (Ctd); 11 oxygens, Σcations − Na − K = 7 − Ti (Bt); 11 oxygens, Σcations − Na − K = 6 (Pg, Phe); 12·5 oxygens (Czo).

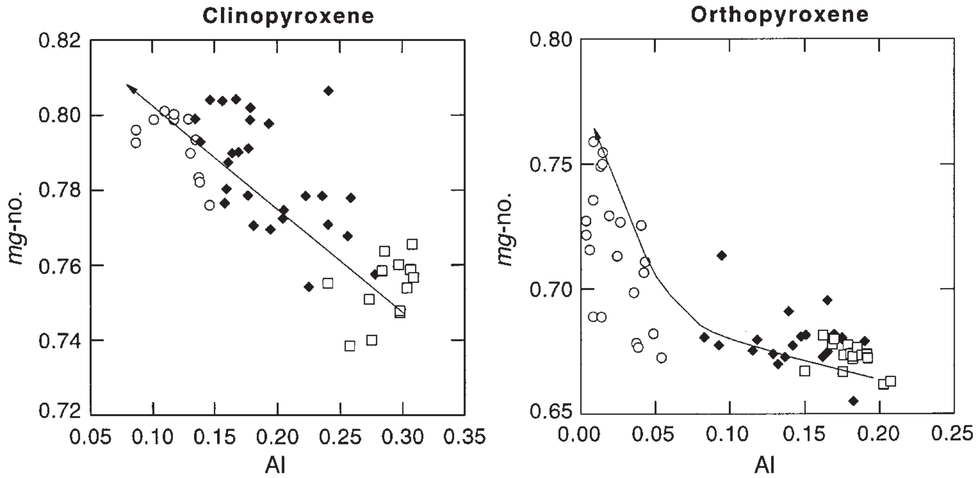


**Fig. 6.** Mineral composition of clinopyroxene and orthopyroxene in sample B-F 7. The Al content of pyroxene (cations per formula unit) decreases with increasing *mg*-number. □, coarse granular (primary) pyroxene; ◆, pyroxene related to spinel–two-pyroxene corona; ○, pyroxene related to garnet–two-pyroxene corona.

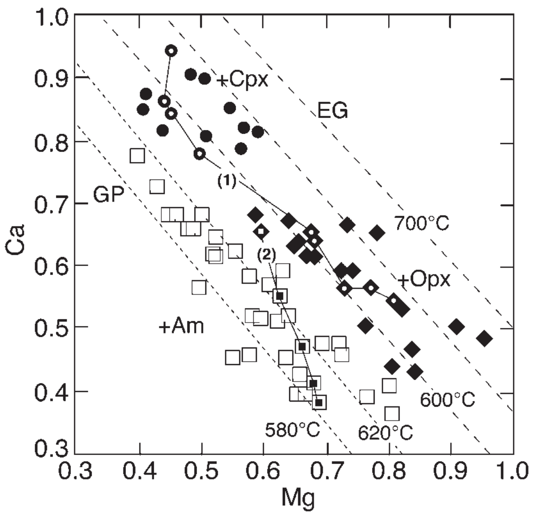


**Fig. 7.** Garnet composition in sample B-F 7. Mg-rich garnet grains are in textural equilibrium with orthopyroxene (◆), whereas garnet grains in textural equilibrium with clinopyroxene (●) show higher Ca contents. Garnet grains that coexist with amphibole (□) have a higher almandine component and correspondingly lower Ca and Mg. Continuous line connects points from probe traverses through corona garnet: (1) garnet between clino- and orthopyroxene; (2) garnet between orthopyroxene and amphibole. Isotherms are calculated with the Ellis & Green (1979) thermometer using clinopyroxene $Cpx_3$ (Table 4) for the garnet granulites (EG, long-dashed lines). Garnet amphibolite isotherms are calculated with the Graham & Powell (1984) thermometer using $Am_1$ (Table 4) as coexisting amphibole (GP, short-dashed lines).

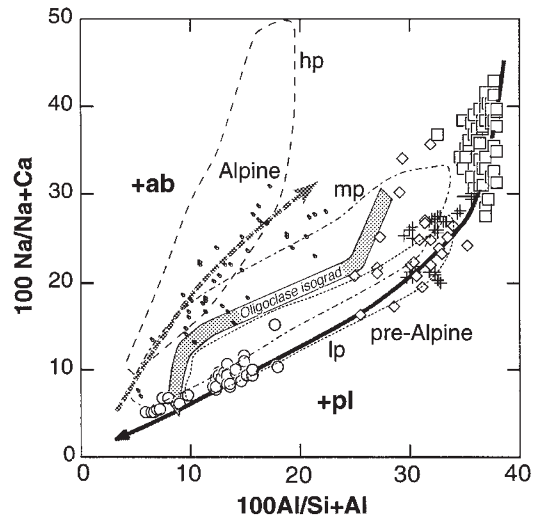


**Fig. 8.** Compositional variation of amphibole, after Laird & Albee (1981). The fields of 'high-pressure amphiboles' (hp, dashed line), 'medium-pressure amphiboles' (mp, dashed–dotted line) and 'low-pressure amphiboles' (lp, dotted line) are indicated. Amphiboles from different retrograde stages (□, garnet amphibolite coronas; ◇, biotite amphibolite coronas; ○, pseudomorphic textures) plot in the plagioclase field. Amphibole grown during Alpine metamorphism (●) is given for comparison. The 'oligoclase isograd' (Laird & Albee, 1981) separates pre-Alpine from Alpine amphibole. +, Amphiboles grown during Oligocene contact metamorphism.

## Malenco peridotite

Metamorphic clinopyroxene exhibits a two-fold decrease in Al and a two- to four-fold decrease in Cr and Ti compared with the primary mantle assemblages (Müntener, 1997). Orthopyroxene shows a two-fold decrease in Al with respect to its mantle counterpart. Iron/magnesium ratios vary with bulk-rock composition, coexisting minerals and temperature. For example, the $K_D^{Fe-Mg}$ between olivine and clinopyroxene increases from spinel peridotite assemblages to granulite-facies

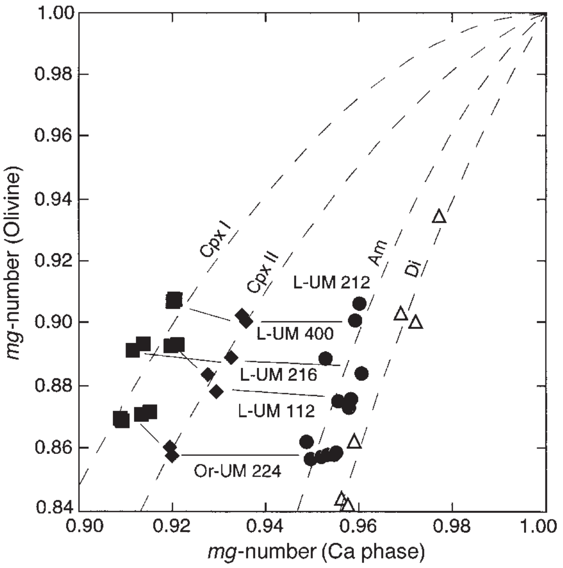


**Fig. 9.** Distribution of Mg and Fe between olivine and coexisting Ca phases during pre-Alpine retrograde metamorphism of the Malenco ultramafic rocks. ■, Olivine and clinopyroxene porphyroclasts; ◆, olivine II and clinopyroxene granoblasts; ●, olivine III and tremolite; △, olivine and diopside of Alpine metamorphic assemblages (Trommsdorff & Evans, 1972). Dashed lines are third-order polynomial fits, which pass through the origin and the point (1,1). Minerals from the same sample are connected with a line. Samples L-UM 112, 212, 216 and 400 are 'granular' peridotites with little pre-Alpine retrograde recrystallization, and sample Or-UM 224 is a porphyroclastic peridotite, strongly recrystallized to amphibolite-facies parageneses.

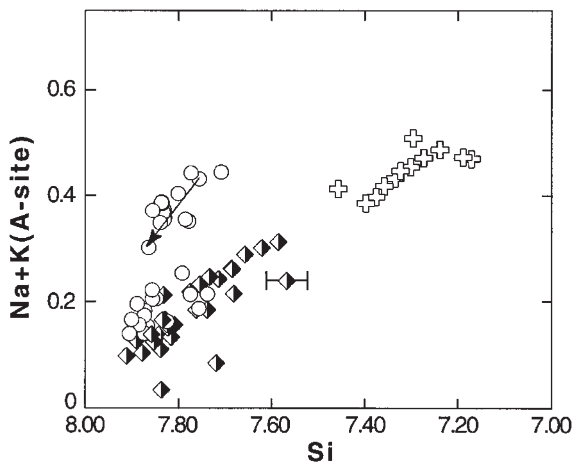


**Fig. 10.** Compositional variation of amphibole in Malenco ultramafic rocks. Open crosses, Mg-hornblende interstitial to olivine and pyroxenes; half-shaded diamonds, tremolite pseudomorphs after clino- and orthopyroxene; ○, dynamically recrystallized tremolite in pressure shadows of clinopyroxene porphyroclasts. Arrow indicates core-to-rim zoning. (See text for discussion.)

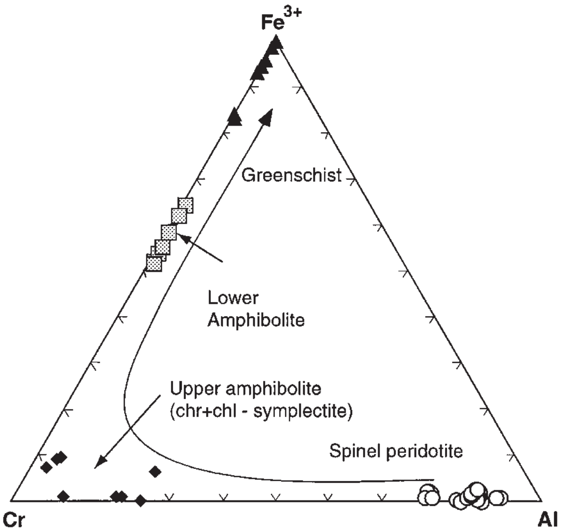


**Fig. 11.** Spinel composition in the ternary diagram Al, Cr and $Fe^{3+}$. Spinel composition changes from Al rich to Cr rich during the transition from granulite (spinel peridotite) facies to upper amphibolite facies conditions. During further retrograde metamorphism ferrichromite is stable with olivine, amphibole and Cr-rich chlorite. Magnetite formed at low-grade conditions, and during Alpine, greenschist-facies metamorphism.

neoblasts (Fig. 9). During the transition from clinopyroxene to amphibole, the Fe/Mg of associated olivine remains constant.

Amphibole formed during retrograde metamorphism varies from Mg-hornblende to tremolite (Fig. 10). It is present as corona grains, as pseudomorphs after pyroxene or as dynamically recrystallized grains in the pressure shadows of pyroxene porphyroclasts. In the last case it is Na-rich, Al-poor tremolite (Table 5). The high calculated $Na^{(M4)}$ of dynamically recrystallized amphibole is not balanced by trivalent octahedral cations, but by extra Na + K on the A-site (Fig. 10), indicative of a richterite substitution $Na^{A}Na^{M4}Ca^{M4}{}_{-1}$, and possibly recording relatively high pressure during retrograde metamorphism.

The compositions of spinel correlate with decreasing metamorphic grade. The granulite to amphibolite transition is dominated by the exchange $FeCr(MgAl)_{-1}$ (Fig. 11), but $TiO_2$ and MnO increase and NiO decrease (Table 5), as a result of equilibrium with chlorite. With more complete retrogression the spinel is ferrichromite, and coexisting chlorite becomes richer in Cr. Chlorite that coexists with chromite is distinctly higher in $Al_2O_3$ than chlorite that coexists with amphibole (Table 5). The Al content of chlorite decreases with metamorphic grade, and shows an antithetic variation with Cr content (Table 5).

## Metapelites

Part of the mineral compositions of metapelites have already been published by Hermann *et al.* (1997) and are reported here for completeness of the retrograde metamorphic evolution (Table 6). The change in garnet composition is the best documentation for retrograde metamorphism in the metapelites. High-pyrope garnets ($Py_{37}$) have composite rims of grt2 and grt3. Grt2 is characterized by a decrease in Mg at constant grossular content. The transition to grt3 is marked by a significant Ca increase. Small neoblastic garnets in the matrix have grt3 composition and are also zoned, with an increase in Ca towards the rim (grt4). In the hydrous corona between kyanite and garnet, rare grains of staurolite and chloritoid record *mg*-number$_{ctd}$ > *mg*-number$_{grt}$ > *mg*-number$_{stau}$.

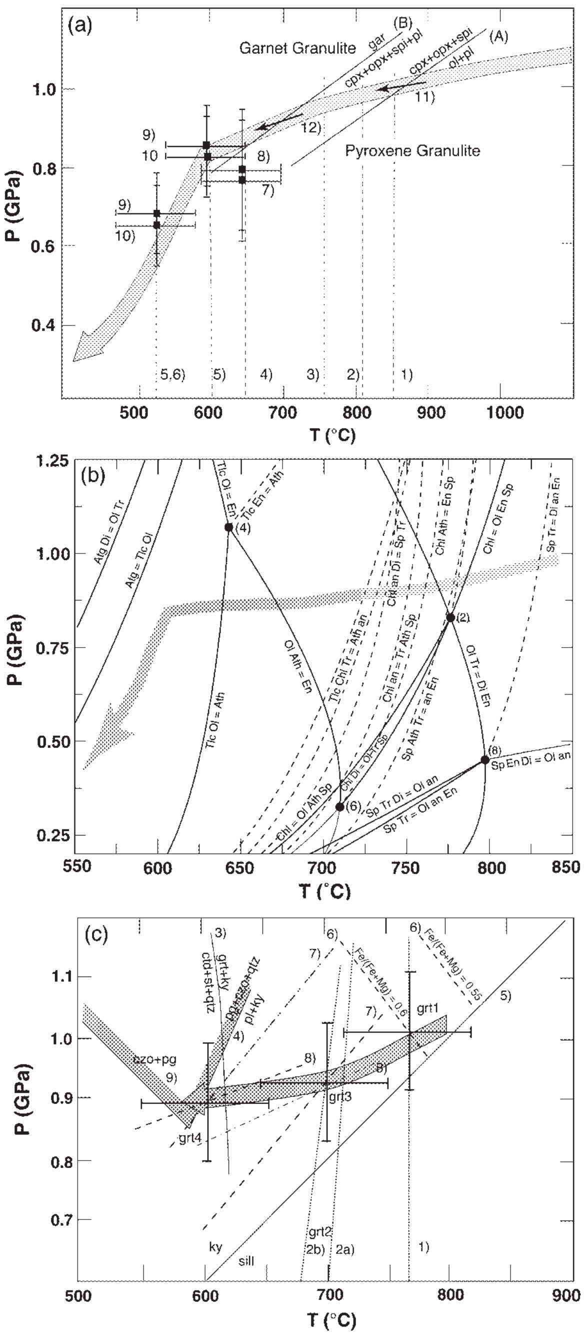


## Summary of microstructures and mineral chemistry

Combining all petrographic and mineral chemistry data, the microstructures suggest that anhydrous recrystallization in all rock types preceded widespread hydrous recrystallization, and that the Malenco rocks underwent two successive metamorphic *P–T* paths. The first of these was dominated by near-isobaric cooling under anhydrous conditions, which is best documented in the gabbros and granulitic metapelites. Pyroxene composition is related to the transition from olivine gabbro through spinel to garnet granulite, which is characteristic of isobarically cooled gabbros (e.g. Whitney & McLelland,

**Fig. 12.** *P–T* diagrams for the mafic, ultramafic and pelitic rocks of the Malenco area. Estimated errors are $\pm 50$°C, $\pm 0{\cdot}1$ GPa for exchange thermometers and barometers, and $\pm 25$°C for net transfer reactions. (a) Compiled *P–T* diagram for the Braccia gabbro. Temperatures: (1) Caroll Webb & Wood (1986); (2) Wood & Banno (1973); (3) Wells (1977); (4) Ellis & Green (1979); (5) Graham & Powell (1984); (6) Pownceby *et al.* (1987). Pressures: (7) Newton & Perkins (1982); (8) Moecher *et al.* (1988); (9) Kohn & Spear (1989) (Mg); (10) Kohn & Spear (1989) (Fe); (11) Herzberg (1978); (12) Ito & Kennedy (1971). The reaction curves A and B qualitatively show the transition from ol + pl through spinel to garnet granulite. (b) Petrogenetic grid for a portion of the system $CaO–FeO–MgO–Al_2O_3–SiO_2–H_2O$, calculated with Vertex (Connolly 1990), using the database of Berman (1988) for the minerals antigorite (Atg), olivine (Ol), enstatite (En), anthophyllite (Ath), talc (Tlc), chlorite (Chl), anorthite (An), diopside (Di), tremolite (Tr) and spinel (Sp). (Note different scale on *T* axis.) Water activity was assumed to be unity. Additional calculations (not shown) with $a_{H_2O} = 0{\cdot}5$ result in a temperature decrease of $\sim 50$°C for reactions involving $H_2O$, but leave the topology unchanged. Dashed curves correspond to olivine-absent reactions. Phase relations involving garnet are not shown. Curves are labeled by the appropriate reaction equations, with the high-temperature assemblage on the right. *mg*-numbers used in the calculation as listed in Table 5. The *mg*-number of anthophyllite is 0·88, typical of retrogressed ultramafic rocks from the Central Alps. The arrow corresponds to retrograde metamorphism of the Malenco ultramafic rocks. The breakdown of orthopyroxene to olivine + talc ± chlorite ± tremolite instead of anthophyllite indicates relatively high pressure during retrograde hydration. (c) *P–T* diagram for Malenco metapelites, modified after Hermann *et al.* (1997). Temperatures: (1) Grt–Ilm (Pownceby *et al.*, 1987); (2) Grt–Bt: (a, Hodges & Spear, 1982; b, Ferry & Spear, 1978); (3) Grt + Ky + $H_2O$ → Ctd + St + Qtz and (4) Pl + Ky + $H_2O$ → Pg + Czo + Qtz, both calculated with Vertex (Connolly, 1990) with database of Holland & Powell (1990). Pressures: (5) Ky–Sil (Holdaway, 1971); (6) Fe–Mg in Grt (Spear & Cheney, 1989); (7) GASP (Ghent, 1976) with parameters of Newton & Haselton (1981); (8) GRIPS (Bohlen & Liotta, 1986) with parameters of Hodges & Spear (1982) and Hodges & Royden (1984); (9) stability field of czo + pg, calculated with Vertex (Connolly, 1990) with database of Holland & Powell (1990). Grt 1–4 as given in Table 6. Shaded band outlines stability field for the paragenesis Czo + Pg. Shaded arrow indicates *P–T* path of metapelites.

1973; Bohlen, 1987; Johnson & Carlson, 1990). Near-isobaric cooling is also documented in the metapelites by recrystallization of kyanite, the increase of grossularite content of garnet that coexisted with plagioclase and kyanite, and the transition of ilmenite to rutile (Bohlen & Liotta, 1986). The ultramafic rocks recrystallized from spinel to chlorite peridotite, above the spinel- to plagioclase-facies transition, which is consistent with cooling at only a moderate pressure decrease. The subsequent retrograde metamorphism is characterized by near-isothermal decompression under hydrous conditions. Hydration reactions in all rocks partly overprinted the anhydrous assemblages. Variations in composition of amphibole in the presence of plagioclase ($An_{30-40}$) in mafic rocks (Laird & Albee, 1981), and the stability of olivine + tremolite in ultramafic rocks (see Fig. 12b below) are the most reliable indicators for decompression at temperatures of the amphibolite facies.

One of the most serious drawbacks for a quantitative determination of retrograde metamorphism is the lack of complete re-equilibration of the rocks. Despite this, chemical equilibrium was probably approached at contacting grain boundaries in coronas that show textural equilibrium, but obviously not at the scale of a whole thin section. This is shown by the chemical zoning of garnets in metagabbros (Fig. 8) as discussed below. However, Johnson & Carlson (1990) have shown that coronas probably maintain local equilibrium, and therefore *P–T* estimates on the basis of corona mineral chemistry can be obtained. In the following discussion, we present *P–T* estimates by combining relevant mineral chemistry information with conventional thermobarometers from all three rock types.

## *P–T* ESTIMATES FROM MINERAL CHEMISTRY

The following *P–T* estimates for the Malenco rocks were obtained and are compiled in Fig. 12a–c (see caption for references):

(1) the gabbro crystallized at 1·0–1·2 GPa and 1150–1250°C. This estimate is based on the magmatic assemblages of plagioclase, pyroxenes, Al-rich spinel and olivine. The temperatures are close to the dry solidus of basalt (1200–1300°C; Green & Ringwood, 1967).

(2) Granulite-facies conditions are recorded by all three rock types, and are estimated as 750–850°C and 0·9–1·1 GPa. Temperature estimates in the gabbros are based on spinel–pyroxene coronas and coexisting pyroxenes. Orthopyroxene–olivine–spinel thermometry (Caroll Webb & Wood, 1986) yields a temperature of ~850°C, about 300°C lower than that for 'primary' grains. Two-pyroxene thermometry, applied to both groundmass and corona grains, yields values around 800°C. Over the temperature difference of more than 300°C between the formation of 'primary' minerals and of anhydrous corona grains, the Braccia gabbro maintained the five-phase assemblage ol + pl + cpx + opx + spl. This assemblage has a limited pressure stability of 1·0–1·35 GPa (e.g. Green & Ringwood, 1967). At lower pressures, olivine and plagioclase are stable instead of clinopyroxene, orthopyroxene and spinel, and at higher pressures, garnet + olivine should be present, which is not the case. This suggests that between the temperatures of intrusion (~1150–1250°C) and of spinel + pyroxene corona formation (~800–850°C), the olivine gabbros cooled nearly isobarically within the five-phase stability field. Pyroxene and spinel compositions changed towards CMAS and MAS end members, respectively (Fig. 6), which is also consistent with isobaric cooling.

Orthopyroxene–spinel–olivine (Caroll Webb & Wood, 1986) and two-pyroxene thermometry (Brey & Köhler, 1990) for the peridotites record a temperature of 750 ± 50°C, which is about 200°C lower than the temperature obtained from large porphyroclastic mantle minerals (Müntener, 1997). This temperature overlaps with those estimated for the granulite-facies metamorphism of metapelites (Hermann *et al.*, 1997), but is slightly lower than those obtained from the gabbros.

At temperatures of 800 ± 50°C, pressure estimates for the granulite-facies metamorphism are constrained by the presence of kyanite and the composition of garnet in the pelitic granulites to about 0·9–1·1 GPa (Hermann *et al.*, 1997).

(3) The *P–T* estimates for the last anhydrous equilibration are based on mineral equilibria in metapelites and metagabbros and are estimated as 550–650°C and 0·7–0·9 GPa. For the garnet + clinopyroxene coronas in the metagabbros, the Ellis & Green (1979) thermometer yields temperatures between 660 and 600°C (Fig. 7) within one sample. Although the garnets display a large compositional variation depending on the microstructural site, calculated temperatures cover a restricted range (Fig. 7). From this we suggest that local equilibrium was achieved. A similiar temperature of 580–640°C has been calculated for sample L-F 107, which has a higher bulk *mg*-number. Because the amount of $Fe^{3+}$ in clinopyroxene was not determined, calculated temperatures might be several tens of degrees on the high side (i.e. ~20°C for $Fe^{3+}/Fe_{tot}$ = 0·1). Olivine–spinel thermometry in peridotites yields equilibration temperatures of 600 ± 50°C, which overlap with those obtained from metagabbros.

In the metapelites the assemblage garnet–kyanite–plagioclase–quartz (GASP, Ghent, 1976) indicates pressures of 0·8–1·0 GPa at 600°C, using grt4, pl2, and unit activity for kyanite and quartz. The formation of garnet–pyroxene coronas in mafic rocks is consistent with the pressures obtained from the metapelites. The equilibrium among garnet, plagioclase, orthopyroxene and $SiO_2$ can be used here to estimate only maximum pressures because the activity of $SiO_2$ is <1. The calibrations of Newton & Perkins (1982) and of Moecher *et al.* (1988) both give similar maximum pressures of about 0·8 ± 0·15 GPa, at 650°C.

(4) Isotherms calculated for garnet + amphibole coronas in metagabbros (Graham & Powell, 1984) yield a temperature of 600 ± 20°C, somewhat lower than for the garnet + pyroxene coronas. A temperature of 610°C for the hydration in the metapelites was calculated from the equilibrium involving garnet, kyanite, chloritoid, staurolite and quartz, which is univariant in FMASH. A temperature of ~600°C, for the equilibrium reaction of kyanite, plagioclase, clinozoisite, paragonite and quartz, was calculated for the hydration of plagioclase in kyanite-bearing metapelites.

A temperature estimate of ~600°C is consistent with olivine + talc replacement of orthopyroxene in ultramafic rocks. These temperatures are considerably lower than those calculated for ol + en + spl → chl and opx + cpx → ol + tr in Fig. 12b. Olivine–spinel thermometry (e.g. O'Neill & Wall, 1987), on the other hand, indicates that cooling under anhydrous conditions reached ~600°C, consistent with data from metagabbros and metapelites. We conclude that major hydration in the Malenco peridotite took place at temperatures of less than ~600°C, within the stability of olivine + talc.

The pressure of formation of the first hydrous assemblage is constrained by the paragenesis clinozoisite + paragonite in metapelites, which indicates a minimum pressure of 0·85 GPa (Fig. 12c). The compositions of garnet, staurolite and chloritoid coexisting with kyanite and quartz are consistent with 0·8–1·0 GPa for the hydration, in agreement with the stability of clinozoisite and paragonite. A maximum pressure in the metagabbros was estimated with the garnet–amphibole–plagioclase–quartz barometer (Kohn & Spear, 1989). Both Fe and Mg end-member calibrations give maximum pressures of about 0·85 ± 0·1 GPa (again, $a_{SiO_2}$ <1). However, a similar $a_{SiO_2}$ can be considered for garnet–pyroxene and garnet–amphibole coronas in olivine gabbros, because the minerals involved display contacts with each other. This results in similar pressure estimates for garnet–pyroxene and garnet–amphibole coronas. In summary, the *P–T* data for the first hydration are constrained at ~600°C, 0·8–1·0 GPa and overlap with those of the last anhydrous re-equilibration [point (3) above].

(5) Indications of near-isothermal decompression are based on mineral equilibria in biotite–amphibole–garnet–ilmenite coronas. A temperature for this event was calculated by garnet–ilmenite (Pownceby *et al.*, 1987) and garnet–amphibole (Graham & Powell, 1984) thermometers as 525 ± 50°C. The pressure was constrained by the assemblage garnet–amphibole–plagioclase–quartz (Kohn & Spear, 1989), which indicates a maximum pressure of 0·6 ± 0·2 GPa. Despite the large uncertainties, the *P–T* data are at least good qualitative indications for the *P–T* evolution. The coexistence of plagioclase and amphibole indicates that retrogression occurred under amphibolite-facies conditions. The change of amphibole composition reflects decompression (Fig. 8). Compositions of amphibole from garnet amphibolite samples overlap with values for the 'medium-pressure field' of Laird & Albee (1981), whereas those from biotite amphibolite samples are lower in Na(M4) and overlap the 'low-pressure field' of Laird & Albee (1981). The presence of plagioclase indicates that temperatures are higher than ~520°C (the 'oligoclase isograd'), and thus exceed the maximum temperatures that were reached during Alpine metamorphism under which albite was stable (Fig. 8). In ultramafic rocks olivine and tremolite were stable during the retrograde evolution, which is consistent with decompression at temperatures of 500–600°C (Fig. 12b).

### Conclusions from thermobarometry

The estimate of absolute pressure and temperature conditions of the Malenco rocks involves errors that might be large for a single calculation. However, the combination of several thermobarometers from different rock types shows a systematic retrograde metamorphic evolution from granulite-facies to low-grade conditions (Fig. 13). Combining all available data, the following values represent the most likely *P–T* conditions of the Malenco rocks:

(1) intrusion of gabbro: 1·0–1·2 GPa, 1150–1250°C;
(2) granulite-facies equilibration: 0·9–1·1 GPa, 750–850°C;
(3) end of near-isobaric cooling: 0·7–0·9 GPa, 550–650°C;
(4) first hydration: 0·8–1·0 GPa, 550–650°C;
(5) decompression: 0·8 → 0·4 GPa, 500–600°C;
(6) exhumation: <0·1 GPa, <300°C.

## DISCUSSION

The microstructures, mineral chemistry and the derived *P–T* paths reported here allow us to place some constraints on the cooling history and exhumation of the deep crust and continental upper mantle. The transition from anhydrous to hydrous parageneses is a crucial point in the petrogenesis of the Malenco rocks. The *P–T* data indicate that the metamorphic conditions of the last anhydrous equilibration overlap with those of the first hydration. Anhydrous, near-isobaric cooling provides an insight into the thermal evolution of the Adriatic

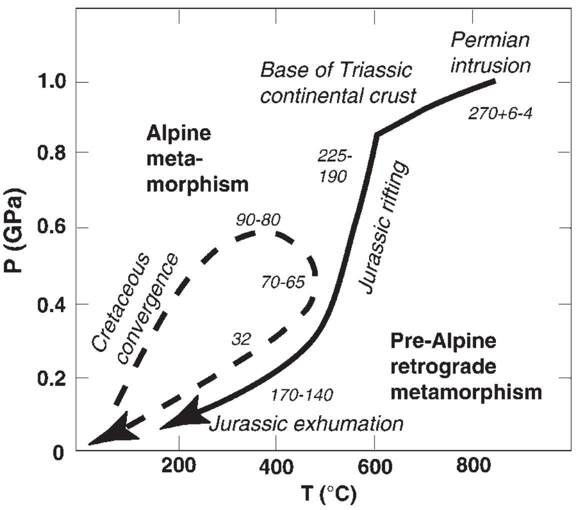


**Fig. 13.** Schematic *P–T–t* diagram for the Malenco crust–mantle complex. Underplating and thermal relaxation are separated by Early Jurassic exhumation and late Jurassic emplacement at the Tethyan ocean floor. During Cretaceous convergence the crust–mantle transition was integrated into the Alpine nappe pile. Final exhumation occurred within the Tertiary and exposed the Permian crust-to-mantle interface. Numbers correspond to age determinations (in Ma). The Braccia gabbro intrusion and the leucosomes in the pelitic granulites have been dated by the U–Pb method in zircons (Hansmann *et al.*, 1996; Hermann *et al.*, 1997). Rifting and exhumation of the crust–mantle transition is constrained by $^{40}Ar/^{39}Ar$ dating of pargasite (Müntener *et al.*, 1997; Villa *et al.*, 2000). Alpine *P–T–t* path: both peak metamorphic pressure and later peak metamorphic temperature are of Cretaceous age, as indicated by Ar–Ar ages of amphibole (Müntener *et al.*, 1997; Villa *et al.*, 2000). The last *P–T–t* point is given by the intrusion of the Oligocene Bergell tonalite at 31·9 ± 0·09 Ma (Von Blanckenburg, 1992).

lithosphere after magmatic underplating in the Permian, whereas the hydrous *P–T* evolution illustrates exhumation metamorphism of the lower crust and upper mantle during continental rifting in Late Triassic–Early Jurassic time.

## Thermal state of the Adria lithosphere

The field relations, U–Pb geochronology, and metamorphic history of the Malenco area reported here indicate the following: (1) underplating of the Braccia gabbro and granulite formation are unrelated to later hydration and exhumation (Fig. 13), which occurred after a time span of >50 My; (2) the Malenco rocks represent the lowermost crust and upper mantle in late Permian and Triassic times; (3) granulite-facies metamorphism in the lower-crustal rocks was caused by the intrusion of the Braccia gabbro (Müntener & Hermann, 1996; Hermann *et al.*, 1997); (4) the end of near-isobaric cooling approached conditions ($P = 0{\cdot}8 \pm 0{\cdot}1$ GPa, $T = 600 \pm 50$°C) that correspond to a thermally undisturbed, stable continental crust. The moderate pressure decrease of $\sim 0{\cdot}2 \pm 0{\cdot}1$ GPa may reflect relaxation after a major period of igneous activity in the Southern and Eastern Alps during the Permian (e.g. Handy & Zingg, 1991; Dal Piaz, 1993; Vavra *et al.*, 1996, 1999). Near-isobaric cooling ended during the Permian, and the resultant conditions at the base of the continental crust persisted into Triassic times.

The detailed *P–T–t* evolution of the Malenco fossil crust-to-mantle transition allows us to contrast isobarically cooled (IBC) and isothermally decompressed (ITD) granulites (Harley, 1989). On the basis of thermal models, Bohlen (1987) proposed that IBC granulites were caused by magmatic underplating and subsequent cooling beneath continental crust. Later he pointed out that the granulite genesis is typically unrelated to exhumation (Bohlen, 1991). IBC granulites have therefore been interpreted to be true lower crust (Rudnick & Fountain, 1995). The Malenco granulites fulfill all the requirements for true lower crust that is in contact with the uppermost continental mantle. The metamorphic conditions ($P = 0{\cdot}8 \pm 0{\cdot}1$ GPa, $T = 600 \pm 50$°C) would correspond to a surface heat flow of $\sim 70\,mW/m^2$ [thermal model of Chapman (1986)]. Such a heat flow is slightly higher than the average value of $60\,mW/m^2$ measured today (Pollack & Chapman, 1977), but may be typical for young continental crust. It is worth while to note that, at the end of the near-isobaric cooling, the metamorphic conditions are of the amphibolite facies. The only reason why some of these rocks remained granulites and spinel peridotites is probably low $H_2O$ activity. If $H_2O$ activity was high, the uppermost subcontinental mantle in regions of $<60\,mW/m^2$ should be retrogressed to chlorite-($\pm$amphibole)-bearing peridotite.

## Exhumation of lower crust and uppermost continental mantle

Near-isothermal decompression and hydration (Fig. 13) occurred while the Malenco complex was exhumed. The decompression was characterized by high $dP/dT$, with about 0·4 GPa between 600°C and 500°C (Figs 12 and 13). *P–T* paths modeled for extension (Chapman & Furlong, 1992) suggest the rates and duration of this unroofing event. Adopting the estimated continental geotherm for the Malenco complex at the end of isobaric cooling, decompression probably took place in 15–30 My. This implies that once rifting started, the exhumation of lower crust and uppermost mantle to upper-crustal levels can occur at exhumation rates of 1–2 mm/year. Such rapid exhumation is qualitatively consistent with the sedimentary record of the Austroalpine margin. Syn-rift sediments of lower Jurassic age formed within a time period of about 20 My (Froitzheim & Eberli, 1990). Hydration during Jurassic rifting is supported by $^{40}Ar/^{39}Ar$ analyses of amphibole, which indicate minimum ages of 190–225 Ma (Müntener *et al.*, 1997). The $^{40}Ar/^{39}Ar$ data and age results of pre-Alpine and Alpine amphiboles have been discussed in detail by Villa *et al.* (2000).

## Do hydration reactions at the base of the continental crust trigger the formation of Cl-rich fluids?

The available data for the Malenco rocks suggest that the $P$–$T$ conditions of the last anhydrous and the first hydrous events overlap. Our study also suggests that the lowermost crust and the uppermost continental mantle can act as fluid sinks. One of the most surprising features is that the first hydration occurred at 0·8–1·0 GPa, which corresponds to the base of a 'normal' continental crust. After a near-isobaric cooling period, the rocks were nearly dry. Later hydration reactions require an external source for fluid. Constraints on the fluid composition are given by phase equilibria in retrogressed peridotite and garnet clinopyroxenite (Müntener, 1997), and retrogressed olivine marble (Hermann, 1997), that indicate an $X\mathrm{CO_2}$ <0·05. Cl contents of amphibole and biotite from coronas in metagabbros vary from 0·2 to 0·63 wt % (Table 4). Because of the high fluid–solid partition coefficient for Cl (Volfinger *et al.*, 1985), the crystallization of Cl-rich phases during the earliest stage of hydration ($P$ = 0·8–1·0 GPa, $T$ = 600 ± 50°C) indicates the presence of highly saline brines in the lowermost crust (and possibly the uppermost continental mantle) during the initial stages of retrograde amphibolite-facies hydration. Irrespective of the mechanism for enrichment of Cl in metamorphic fluids, for example 'fluid unmixing' (Trommsdorff & Skippen, 1986) or 'desiccation' (Kullerud, 1996; Markl & Bucher, 1998), Cl-rich hydrosilicates may be common in granulite terrains that have been partly retrogressed to amphibolite facies.

## Hydration mechanisms

Two alternative external fluid sources seem possible (Fig. 14): (1) lower-crustal fluids could be generated by dehydration reactions in the hanging wall of a major shear zone; (2) fluids might migrate down shear zones from higher levels in the crust, where free fluid phase is present.

The base of the continental crust could become hydrated if such rocks were exhumed along a lithosphere-scale shear zone system (e.g. Lemoine *et al.*, 1987; Vissers *et al.*, 1991; Trommsdorff *et al.*, 1993; Hermann & Müntener, 1996). The almost anhydrous, hotter rocks of the footwall of the shear zone would be progressively brought into contact with cooler, hydrous hanging wall. The near-isothermal decompression indicates that exhumation was faster than thermal equilibration, and thus a thermal gradient existed across the shear zone. Heating of the hanging wall would partly dehydrate its rocks. The fluids released by such a process could enter the shear zone and partially hydrate its footwall.

The alternative for fluid infiltration requires fluid transport down shear zones to the base of the crust (0·8–1·0 GPa). Seismic (or dilatancy) pumping (e.g. Sibson *et al.*, 1975; Fricke *et al.*, 1992; Morrison, 1994) could provide such a mechanism for migration of fluid. It might occur if rocks in shear zones could absorb fluid as a consequence of dilatancy induced by microcracking.

In both cases the introduction of an external fluid and the formation of hydrous phases would favor Cl enrichment in the fluid and strain localization along shear zones.

## Implications for rifting

Many have proposed that in the Alps, late Permian extension and concomitant magmatism evolved to continental rifting in the Mesozoic (e.g. Dal Piaz *et al.*, 1977; Piccardo *et al.*, 1990; Dal Piaz, 1993; Trommsdorff *et al.*, 1993; Rampone *et al.*, 1995). However, a $P$–$T$ path with near-isobaric cooling, followed by Jurassic near-isothermal decompression, is incompatible with continuous crustal extension from the Permian to the middle Jurassic. Permian extension and Jurassic rifting must have been two clearly different tectonic events. This has important implications for the retrograde metamorphism of the peridotitic rocks. In the Alpine realm, a non-adiabatic high-temperature evolution of subcontinental peridotite has been interpreted to represent the incipient rifting that culminated in the emplacement of lithospheric mantle on the floor of the Tethyan ocean (Vissers *et al.*, 1991; Hoogerduijn Strating *et al.*, 1993; Rampone *et al.*, 1995). Our data indicate that rifting is recorded by the retrograde hydration of peridotites, whereas the anhydrous high-temperature reactions in peridotite reflect one or several older events.

Metagabbros and pelitic granulites that were exhumed together with subcontinental mantle may help us to better understand the significance of granulite-facies rocks along passive continental margins. The $P$–$T$ estimates for the Malenco granulites before rifting correspond to amphibolite-facies conditions. They are granulites only because of mafic underplating ~50 My before continental rifting. However, in areas without mafic underplating, the lowermost continental crust may consist of amphibolite-facies rocks that are indistinguishable from upper-crustal basement rocks. On the other hand, as pointed out by Harley (1989) and Rudnick & Fountain (1995), not all exhumed granulites represent the lowermost continental crust. For example, zircon fission track ages of granulites

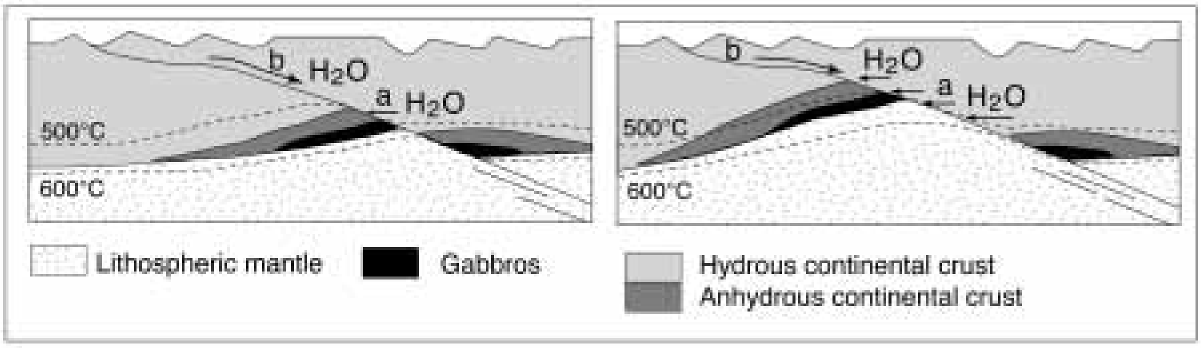


**Fig. 14.** Schematic model for the hydration of the lithospheric mantle and associated lower crust. (a) Hydration caused by dehydration reactions in the hanging wall. (b) Hydration caused by fluid ingress along detachment faults. (See text for discussion.)

from the continent–ocean transition of the Galicia margin indicate that these rocks were already at upper-crustal levels before rifting (Fügenschuh *et al.*, 1998) and most probably do not represent true lower crust. Granulite-facies rocks from the Valpelline series and the Sesia zone in the Western Alps (Lardeaux & Spalla, 1991; Gardien *et al.*, 1994) show a *P–T* path with near-isothermal decompression at much higher temperature than the Malenco granulites. Because Gardien *et al.* (1994) favored a late Variscan formation of the Valpelline granulites as a result of post-collisional thinning, the exhumation of these granulites is not related to Jurassic passive rifting. These examples demonstrate that the presence of granulite-facies rocks alone is not proof of exhumation of the lowermost crust during rifting, even though these rocks are in an Alpine tectonic position similar to the Malenco granulites.

The hydration of the studied rocks at great depth can best be explained by a shear zone cutting across the whole continental crust (Fig. 14). The presence of mylonites in pre-Alpine high-grade rocks exposed in the Alps (Liguria: Vissers *et al.*, 1991; Ivrea zone: Hodges & Fountain, 1984; Handy & Zingg, 1991; Malenco–Margna: Hermann & Müntener, 1996) suggests localized deformation in the lower crust and upper mantle during Jurassic rifting. The Malenco lower-crust and upper-mantle rocks were probably exhumed along localized shear zones rather than by ductile stretching of the lower crust (e.g. Froitzheim & Manatschal, 1996).

## CONCLUSIONS

The Malenco rocks are unique in representing an intact fossil crust–mantle transition (Hermann *et al.*, 1997). The section consists of, from bottom to top: ultramafic mantle; a metagabbro complex; melt-depleted, metapelitic lowermost continental basement rocks of sub-Moho densities; and normal density crustal rocks. The Malenco complex displays a two-stage metamorphic history in post-Variscan, pre-Alpine time. During the first, Permian, stage the crust–mantle transition was stabilized. In the second, Jurassic, stage it was exhumed. First-stage, anhydrous, granulite-facies mineral assemblages formed in ultramafic, mafic and metapelitic rocks as a response to Permian, mafic magma underplating. These assemblages then cooled isobarically to 600–650°C at the base of an ~30 km thick crust. As a consequence of reduced $H_2O$ activity, the granulitic mineral assemblages remained stable at temperature conditions normally assigned to the amphibolite facies. The Malenco crust–mantle suite remained at these conditions for ~50 My.

The onset of the second stage of metamorphism is characterized by the formation of Cl-rich amphibole and other hydrous phases triggered by external fluid input. This stage started with strong decompression at temperatures of 600–500°C and successive hydration of the Malenco rocks. Fluid for hydration was generated through juxtaposition of relatively hot granulite with dehydrating cooler continental crust, or was infiltrated by seismic pumping. Both mechanisms were facilitated by shear zones that may cut through the entire continental crust into the uppermost continental mantle, for which evidence has been presented by Trommsdorff *et al.* (1993) and by Hermann and Müntener (1996).

It appears that the Austroalpine margin of the Alps is an excellent case study for non-volcanic passive rifting, because both metamorphic constraints on the exhumation of lower-crust and mantle rocks and sedimentological and kinematic data (e.g. Froitzheim & Eberli, 1990; Froitzheim & Manatschal, 1996) are available for the same margin. Estimated uplift rates of 1–2 mm/year for the Malenco complex strongly support sedimentologic investigations of the Austroalpine margin that indicate rifting was a fast process and possibly acted no longer than ~15–30 My. A continuous extensional evolution from the Permian to the Middle Jurassic is unlikely.

## ACKNOWLEDGEMENTS

G. Manatschal, N. Froitzheim, D. Bernoulli, G. B. Piccardo, M. Scambelluri and E. Rampone were constantly encouraging and dubious, which helped to clarify many concepts and ideas presented in this study. We thank E. Reusser and J. A. D. Connolly for their help. We also thank an anonymous reviewer, Dexter Perkins, Ron Frost and Sorena Sorensen for their careful and insightful reviews. We acknowledge financial support provided by Swiss National Science Foundation grants 2000-037388·93/1 and 21-36113·92. One of us (O.M.) acknowledges the support of the Schweizerischer Nationalfonds ('Nachwuchsstipendium') and the Woods Hole Oceanographic Institution during final preparation of the manuscript.

## REFERENCES

Berman, R. G. (1988). Internally consistent thermodynamic data for minerals in the system $Na_2O$–$K_2O$–CaO–MgO–FeO–$Fe_2O_3$–$SiO_2$–$TiO_2$–$H_2O$–$CO_2$. *Journal of Petrology* **29**, 445–522.

Bohlen, S. R. (1987). Pressure–temperature–time paths and a tectonic model for the evolution of granulites. *Journal of Geology* **95**, 617–632.

Bohlen, S. R. (1991). On the formation of granulites. *Journal of Metamorphic Geology* **9**, 223–229.

Bohlen, S. R. & Liotta, J. J. (1986). A barometer for garnet amphibolites and garnet granulites. *Journal of Petrology* **27**, 1025–1034.

Boillot, G., Beslier, M. O., Krawczyk, C. M., Rappin, D. & Reston, T. J. (1995). The formation of passive margins: constraints from the crustal structure and segmentation of the deep Galicia margin, Spain. In: Scrutton, R. A. (ed.) *The Tectonics, Sedimentation and Palaeoceanography of the North Atlantic Region. Geological Society, London, Special Publication* **90**, 71–91.

Brey, G. P. & Köhler, T. (1990). Geothermobarometry in four-phase lherzolites II. New thermobarometers, and practical assessment of existing thermobarometers. *Journal of Petrology* **31**, 1353–1378.

Burkhard, D. J. M. & O'Neill, J. (1988). Contrasting serpentinization processes in the Eastern Central Alps. *Contributions to Mineralogy and Petrology* **99**, 498–506.

Caroll Webb, S. A. & Wood, B. J. (1986). Spinel pyroxene–garnet relationships and their dependence on Cr/Al ratio. *Contributions to Mineralogy and Petrology* **92**, 471–480.

Chapman, D. S. (1986). Thermal gradients in the continental crust. In: Dawson, J. B., Carswell, D. A., Hall, J. & Wedepohl, K. H. (eds) *The Nature of the Lower Continental Crust. Geological Society, London, Special Publication* **24**, 63–70.

Chapman, D. S. & Furlong, K. P. (1992). Thermal state of the lower continental crust. In: Fountain, D. M., Arculus, R. & Kay, R. W. (eds) *Continental Lower Crust*. Amsterdam: Elsevier, pp. 179–199.

Connolly, J. A. D. (1990). Calculation of multivariable phase diagrams: an algorithm based on generalized thermodynamics. *American Journal of Science* **290**, 666–718.

Dal Piaz, G. V. (1993). Evolution of Austro-Alpine and upper Penninic basement in the northwestern Alps from Varican convergence to post-Variscan extension. In: Von Raumer, J. F. & Neubauer, F. (eds) *The Pre-Mesozoic Geology of the Alps*. Berlin: Springer Verlag, pp. 327–344.

Dal Piaz, G. V., De Vecchi, G. P. & Hunziker, J. C. (1977). The Austroalpine layered gabbros of the Matterhorn and Mt. Collon–Dents de Berol. *Schweizerische Mineralogische und Petrographische Mitteilungen* **57**, 59–88.

Ellis, D. J. & Green, D. H. (1979). An experimental study of the effect of Ca upon garnet–clinopyroxene Fe–Mg exchange equilibria. *Contributions to Mineralogy and Petrology* **71**, 13–22.

Ferry, J. M. & Spear, F. S. (1978). Experimental calibration of the partitioning of Fe and Mg between biotite and garnet. *Contributions to Mineralogy and Petrology* **66**, 113–117.

Fountain, D. M. (1989). Growth and modification of lower continental crust in extended terrains: the role of extension and magmatic underplating. In: Mereu, R. F., Müller, S. & Fountain, D. M. (eds) *Properties and Processes of Earth's Lower Cruist. American Geophysical Union Monograph* **51**, 287–299.

Fricke, H. C., Wickham, S. M. & O'Neill, J. R. (1992). Oxygen and hydrogen isotope evidence for meteoric water infiltration during mylonitization and uplift in the Ruby Mountains–East Humboldt range core complex, Nevada. *Contributions to Mineralogy and Petrology* **111**, 203–221.

Froitzheim, N. & Eberli, G. P. (1990). Extensional detachment faulting in the evolution of a Tethys passive continental margin, Eastern Alps, Switzerland. *Geological Society of America Bulletin* **102**, 1297–1308.

Froitzheim, N. & Manatschal, G. (1996). Kinematic model for Jurassic rifting, mantle exhumation, and passive margin formation in the Austroalpine and Penninic nappes (Eastern Switzerland). *Geological Society of America Bulletin* **108**, 1120–1133.

Fügenschuh, B., Froitzheim, N. & Boillot, G. (1998). Cooling history of granulite samples from the ocean–continent transition of the Galicia margin: implications for rifting. *Terra Nova* **10**, 96–100.

Gardien, V., Reusser, E. & Marquer, D. (1994). Pre-Alpine metamorphic evolution of the gneisses from the Valpelline series (Western Alps, Italy). *Schweizerische Mineralogische und Petrographische Mitteilungen* **74**, 489–502.

Ghent, E. D. (1976). Plagioclase–garnet–$Al_2SiO_5$–quartz: a potential geobarometer–geothermometer. *American Mineralogist* **61**, 710–714.

Graham, C. M. & Powell, R. (1984). A garnet–hornblende geothermometer: calibration, testing and application to the Pelona schist, Southern California. *Journal of Metamorphic Geology* **2**, 13–31.

Green, D. H. & Ringwood, A. E. (1967). The genesis of basaltic magmas. *Contributions to Mineralogy and Petrology* **15**, 103–190.

Griffin, W. L. & Heier, K. S. (1973). Petrological implications of some corona structures. *Lithos* **6**, 315–335.

Guntli, P. & Liniger, M. (1989). Metamorphose in der Margna-Decke im Bereich Piz da la Margna und Piz Fedoz (Oberengadin). *Schweizerische Mineralogische und Petrographische Mitteilungen* **69**, 289–301.

Handy, M. R. & Zingg, A. (1991). The tectonic and rheological evolution of an attenuated cross section of the continental crust: Ivrea crustal section, southern Alps, northwestern Italy and southern Switzerland. *Geological Society of America Bulletin* **103**, 236–253.

Hansmann, W., Hermann, J. & Müntener, O. (1996). U–Pb-Datierung des Fedozer Gabbros, einer Intrusion an der Krusten Mantel Grenze. *Schweizerische Mineralogische und Petrographische Mitteilungen* **76**, 116–117.

Harley, S. L. (1989). The origin of granulites: a metamorphic perspective. *Geological Magazine* **126**, 215–247.

Hermann, J. (1997). The Braccia gabbro (Malenco, Alps). Permian intrusion at the crust to mantle interface and Jurassic exhumation during rifting. Ph.D. Thesis, ETH Zürich.

Hermann, J. & Müntener, O. (1996). Extension-related structures in the Malenco–Margna-system: implications for paleogeography and consequences for rifting and Alpine tectonics. *Schweizerische Mineralogische und Petrographische Mitteilungen* **76**, 501–519.

Hermann, J., Müntener, O., Trommsdorff, V., Hansmann, W. & Piccardo, G.B. (1997). Fossil crust-to-mantle transition, Val Malenco (Italian Alps). *Journal of Geophysical Research* **102**, 20123–20132.

Herzberg, C. T. (1978). Pyroxene geothermometry and geobarometry: experimental and thermodynamic evaluation of some subsolidus phase relations involving pyroxenes in the system CaO–MgO–$Al_2O_3$–$SiO_2$. *Geochimica et Cosmochimica Acta* **42**, 945–975.

Hodges, K. V. & Fountain, D. M. (1984). Pogallo line, Southern Alps, northern Italy: an intermediate crustal level, low-angle normal fault? *Geology* **12**, 151–154.

Hodges, K. V. & Royden, L. (1984). Geologic thermobarometry of retrograde metamorphic rocks: an indication of the uplift trajectory of a portion of the northern Scandinavian Caledonides. *Journal of Geophysical Research* **89**, 7077–7090.

Hodges, K. V. & Spear, F. S. (1982). Geothermometry, geobarometry and the $Al_2SiO_5$ triple point at Mt. Moosilauke, New Hampshire. *American Mineralogist* **67**, 1118–1134.

Holdaway, M. J. (1971). Stability of andalusite and the aluminium silicate phase diagram. *American Journal of Science* **271**, 97–131.

Holland, T. J. B. & Powell, R. (1990). An enlarged and updated internally consistent dataset with uncertainties and correlations. *Journal of Metamorphic Geology* **8**, 89–124.

Hoogerduijn Strating, E. H., Rampone, E., Piccardo, G. B., Drury, M. R. & Vissers, R. L. M. (1993). Subsolidus emplacement of mantle peridotites during incipient oceanic rifting and opening of the Mesozoic Tethys (Voltri massif, NW Italy). *Journal of Petrology* **34**, 901–927.

Ito, K. & Kennedy, C. (1971). An experimental study of the basalt–garnet granulite–eclogite transition. In: Heacock, J. G. (ed.) *The Structural and Physical Properties of the Earth's Crust. American Geophysical Union, Geophysical Monograph Series* **14**, 303–314.

Johnson, J. D. & Carlson, W. D. (1990). The origin of olivine–plagioclase coronas in metagabbros from the Adirondack Mountains, New York. *Journal of Metamorphic Geology* **8**, 697–717.

Kohn, M. J. & Spear, F. S. (1989). Empirical calibration of geobarometers for the assemblage garnet + hornblende + plagioclase + quartz. *American Mineralogist* **74**, 77–84.

Kretz, R. (1983). Symbols for rock-forming minerals. *American Mineralogist* **68**, 277–279.

Kullerud, K. (1996). Chlorine-rich amphiboles: interplay between amphibole composition and an evolving fluid. *European Journal of Mineralogy* **8**, 355–370.

Laird, J. & Albee, A. L. (1981). Pressure–temperature and time indicators in mafic schist: their applications to reconstructing the polymetamorphic history of Vermont. *American Journal of Science* **281**, 127–175.

Lardeaux, J. M. & Spalla, M. I. (1991). From granulites to eclogites in the Sesia zone (Italian Western Alps): a record of opening and closure of the Piemont ocean. *Journal of Metamorphic Geology* **9**, 35–59.

Lemoine, M., Tricart, P. & Boillot, G. (1987). Ultramafic and gabbroic ocean floor of the Ligurian Tethys (Alps, Corsica, Apennines). In search of a genetic model. *Geology* **15**, 622–625.

Markl, G. & Bucher, K (1998). Composition of fluids in the lower crust inferred from metamorphic salt in lower-crustal rocks. *Nature* **391**, 781–783.

Mellini, M., Trommsdorff, V. & Compagnoni, R. (1987). Antigorite polysomatism: behaviour during progressive metamorphism. *Contributions to Mineralogy and Petrology* **97**, 147–155.

Moecher, D. P., Essene, E. J. & Anovitz, L. M. (1988). Calculation and application of clinopyroxene–garnet plagioclase–quartz geobarometers. *Contributions to Mineralogy and Petrology* **100**, 92–106.

Montrasio, A. (1973). Strutture a pillow nelle anfiboliti del M. Forno (Penninico medio–Alpi Retichi). *Rendiconti Accademia Nazionale Lincei, Scienzia Fisica Matematica Naturali* **54**, 114–123.

Morrison, J. (1994). Meteoric water–rock interaction in the lower plate of the Whipple Mountain metamorphic core complex, California. *Journal of Metamorphic Geology* **12**, 827–840.

Müntener, O. (1997). The Malenco peridotites (Alps). Petrology and geochemistry of subcontinental mantle and Jurassic exhumation during rifting. Ph.D. Thesis, ETH Zürich.

Müntener, O. & Hermann, J. (1996). The Val Malenco lower crust–upper mantle complex and its field relations (Italian Alps). *Schweizerische Mineralogische und Petrographische Mitteilungen* **76**, 475–500.

Müntener, O., Hermann, J., Villa, I. M. & Trommsdorff, V. (1997). From Jurassic rifting to Cretaceous nappe formation: a combined $^{39}Ar/^{40}Ar$ and microprobe study on amphiboles. *Terra Abstracts* **1**, 489.

Newton, R. C. & Haselton, H. T. (1981). Thermodynamics of the garnet–plagioclase–$Al_2SiO_5$–quartz geobarometer. In: Newton, R. C. (ed.) *Thermodynamics of Minerals and Melts*. New York: Springer Verlag, pp. 131–147.

Newton, R. C. & Perkins, D. I. (1982). Thermodynamic calibration of geobarometers based on the assemblages garnet–plagioclase–orthopyroxene (clinopyroxene)–quartz. *American Mineralogist* **67**, 203–222.

O'Neill, H. St C. & Wall, V. J. (1987). The olivine–orthopyroxene–spinel oxygen geobarometer, the nickel precipitation curve, and the oxygen fugacity of the Earth's upper mantle. *Journal of Petrology* **28**, 1169–1191.

Peretti, A. (1985). Der Monte-del-Forno-Komplex am Bergell-Ostrand: Seine Lithostratigraphie, alpine Tektonik und Metamorphose. *Eclogae Geologica Helvetica* **78**, 23–48.

Piccardo, G. B., Rampone, E. & Vannucci, R. (1990). Upper mantle evolution during continental rifting and ocean formation: evidences from peridotite bodies of the western Alpine–northern Apennine system. *Mémoires de la Société Géologique de France* **156**, 323–333.

Pollack, H. N. & Chapman, D. S. (1977). On the regional variation of the heat flow, geotherms and lithosphere thickness. *Tectonophysics* **38**, 279–296.

Pouchou, J. L. & Pichoir, F. (1984). Un nouveau modèle de calcul pour la microanalyse quantitative par spectrométrie de rayons X. 1. Application à l'analyse d'échantillons homogènes. *Recherches Aerospace* **1984**(3), 167–192.

Pownceby, M. I., Wall, V. J. & O'Neill, H. S. C. (1987). Fe–Mn partitioning between garnet and ilmenite: experimental calibration and applications. *Contributions to Mineralogy and Petrology* **97**, 116–126. (Correction, *Contributions to Mineralogy and Petrology* **97**, 539.)

Pozzorini, D. & Früh-Green, G. L. (1996). Stable isotope systematics of the Ventina ophicarbonate zone, Bergell contact aureole. *Schweizerische Mineralogische und Petrographische Mitteilungen* **76**, 549–564.

Quick, J. E., Sinigoi, S. & Mayer, A. (1995). Emplacement of mantle peridotites in the lower continental crust, Ivrea–Verbano zone, Northwestern Italy. *Geology* **23**, 739–742.

Rampone, E., Hofmann, A. W., Piccardo, G. B., Vanucci, R., Bottazzi, P. & Ottolini, L. (1995). Petrology, mineral and isotope geochemistry of the External Liguride peridotites (Northern Apennines, Italy). *Journal of Petrology* **36**, 81–105.

Rudnick, R. L. & Fountain, D. M. (1995). Nature and composition of the continental crust: a lower-crustal perspective. *Reviews in Geophysics* **33**, 267–309.

Sibson, R. H., Moore, J. M. & Rankin, A. H. (1975). Seismic pumping—a hydrothermal fluid transport mechanism. *Journal of the Geological Society, London* **131**, 653–659.

Spear, F. S. & Cheney, J. T. (1989) A petrogenic grid for pelitic schists in the system $SiO_2$–$Al_2O_3$–FeO–MgO–$K_2O$–$H_2O$. *Contributions to Mineralogy and Petrology* **101**, 149–164.

Trommsdorff, V. & Evans, B. W. (1972). Progressive metamorphism of antigorite schist in the Bergell tonalite aureole. *American Journal of Science* **272**, 423–437.

Trommsdorff, V. & Skippen, G. (1986). Vapour loss ('boiling') as a mechanism of fluid evolution in metacarbonate rocks. *Contributions to Mineralogy and Petrology* **94**, 317–322.

Trommsdorff, V., Piccardo, G. B. & Montrasio, A. (1993). From magmatism through metamorphism to sea floor emplacement of subcontinental Adria lithosphere during pre-Alpine rifting (Malenco, Italy). *Schweizerische Mineralogische und Petrographische Mitteilungen* **73**, 191–203.

Vavra, G., Gebauer, D., Schmid, R. & Compston, W. (1996). Multiple zircon growth and recrystallisation during polyphase Late Carboniferous to Triassic metamorphism in granulites of the Ivrea Zone (Southern Alps): an ion microprobe (SHRIMP) study. *Contributions to Mineralogy and Petrology* **122**, 337–358.

Vavra, G., Schmid, R. & Gebauer, D. (1999). Internal morphology, habit and U–Th–Pb microanalysis of amphibolite-to-granulite facies zircons: geochronology of the Ivrea zone (Southern Alps). *Contributions to Mineralogy and Petrology* **134**, 380–404.

Villa, I. M., Hermann, J., Müntener, O. & Trommsdorff, V. (2000). The $^{39}Ar/^{40}Ar$ dating of multiply zoned amphibole generations (Malenco, Italy) (submitted).

Vissers, R. L. M., Drury, M. R., Hoogerduijn Strating, E. H. & Van Der Wal, D. (1991). Shear zones in the upper mantle: a case study in an Alpine lherzolite massif. *Geology* **19**, 990–993.

Volfinger, M., Robert, J.-L., Vielzeuf, D. & Neiva, A. M. R. (1985). Structural control of the chlorine content of OH-bearing silicates (micas and amphiboles). *Geochimica et Cosmochimica Acta* **49**, 37–48.

Von Blanckenburg, F. (1992). Combined high precision chronometry and geochemical tracing using accessory minerals: applied to the Central-Alpine Bergell intrusion. *Chemical Geology* **100**, 19–40.

Wells, P. R. A. (1977). Pyroxene thermometry in simple and complex systems. *Contributions to Mineralogy and Petrology* **62**, 129–139.

Whitney, P. R. & McLelland, J. M. (1973). Origin of coronas in metagabbros in the Adirondack Mountains, NY. *Contributions to Mineralogy and Petrology* **39**, 81–98.

Wood, B. J. & Banno, S. (1973). Garnet–orthopyroxene and garnet–clinopyroxene relationships in simple and complex systems. *Contributions to Mineralogy and Petrology* **42**, 109–124.